

## **INFORMATION TO USERS**

**This manuscript has been reproduced from the microfilm master. UMI films the text directly from the original or copy submitted. Thus, some thesis and dissertation copies are in typewriter face, while others may be from any type of computer printer.**

**The quality of this reproduction is dependent upon the quality of the copy submitted. Broken or indistinct print, colored or poor quality illustrations and photographs, print bleedthrough, substandard margins, and improper alignment can adversely affect reproduction.**

**In the unlikely event that the author did not send UMI a complete manuscript and there are missing pages, these will be noted. Also, if unauthorized copyright material had to be removed, a note will indicate the deletion.**

**Oversize materials (e.g., maps, drawings, charts) are reproduced by sectioning the original, beginning at the upper left-hand corner and continuing from left to right in equal sections with small overlaps. Each original is also photographed in one exposure and is included in reduced form at the back of the book.**

**Photographs included in the original manuscript have been reproduced xerographically in this copy. Higher quality 6" x 9" black and white photographic prints are available for any photographs or illustrations appearing in this copy for an additional charge. Contact UMI directly to order.**

# **UMI**

**A Bell & Howell Information Company  
300 North Zeeb Road, Ann Arbor MI 48106-1346 USA  
313/761-4700 800/521-0600**



## **NOTE TO USERS**

**The original manuscript received by UMI contains pages with indistinct and/or slanted print. Pages were microfilmed as received.**

**This reproduction is the best copy available**

**UMI**



**ON THE EFFECTS OF INCUDOSTAPEDIAL JOINT FLEXIBILITY  
IN A FINITE-ELEMENT MODEL OF THE CAT MIDDLE EAR**

**Sudeshna S. Ghosh**

**A thesis submitted to the Faculty of Graduate Studies and Research in partial fulfillment  
of the requirements of the degree of Master of Engineering**

**Department of BioMedical Engineering  
McGill University  
Montréal, Canada  
August 1996**

***Copyright Sudeshna S. Ghosh, 1996***



**National Library  
of Canada**

**Acquisitions and  
Bibliographic Services**

395 Wellington Street  
Ottawa ON K1A 0N4  
Canada

**Bibliothèque nationale  
du Canada**

**Acquisitions et  
services bibliographiques**

395, rue Wellington  
Ottawa ON K1A 0N4  
Canada

*Your file* *Votre référence*

*Our file* *Notre référence*

**The author has granted a non-exclusive licence allowing the National Library of Canada to reproduce, loan, distribute or sell copies of this thesis in microform, paper or electronic formats.**

**The author retains ownership of the copyright in this thesis. Neither the thesis nor substantial extracts from it may be printed or otherwise reproduced without the author's permission.**

**L'auteur a accordé une licence non exclusive permettant à la Bibliothèque nationale du Canada de reproduire, prêter, distribuer ou vendre des copies de cette thèse sous la forme de microfiche/film, de reproduction sur papier ou sur format électronique.**

**L'auteur conserve la propriété du droit d'auteur qui protège cette thèse. Ni la thèse ni des extraits substantiels de celle-ci ne doivent être imprimés ou autrement reproduits sans son autorisation.**

0-612-29860-4

## **DEDICATION**

To my parents, Dipti Kumar Ghosh and Sumitra Ghosh, for their constant support and encouragement.

## **ABSTRACT**

A finite-element model of the cat middle ear was modified to include a shell representation of the incudostapedial joint. A low-frequency, uniform sound pressure was applied to the eardrum. Joint stiffness was varied from very low to very high. The resulting displacements of the stapedial footplate, incudostapedial joint, manubrium and eardrum were examined. The footplate tilts both anteroposteriorly and inferosuperiorly for almost all Young's modulus values. The in-plane rotation of the footplate is greatest when the incudostapedial joint is effectively rigid. The joint compresses most when it is extremely flexible and less as the joint becomes less flexible. The joint compression is greater than the joint shear. The displacement pattern of the eardrum is relatively insensitive to changes in the joint stiffness.

## **RÉSUMÉ**

On a modifié un modèle aux éléments finis de l'oreille moyenne du chat, afin d'inclure une représentation à coque mince de l'articulation incudostapédiale. Une pression acoustique uniforme, à basse fréquence, fut appliquée au tympan. La rigidité de l'articulation fut variée entre des valeurs très faibles et des valeurs très élevées. On a examiné les déplacements résultants de la platine stapédiale, de l'articulation incudostapédiale, du manubrium et du tympan. La platine s'incline de façon antéropostérieure et inférosupérieure pour presque toutes les valeurs de rigidité. La rotation dans le plan de la platine est la plus grande lorsque l'articulation incudostapédiale est rigide. L'articulation est comprimée le plus lorsqu'elle est très flexible, et moins quand elle devient moins flexible. La compression de l'articulation est plus importante que sa distorsion latérale. La forme des déplacements du tympan change relativement peu lorsqu'on change la rigidité de l'articulation.

## **ACKNOWLEDGEMENTS**

I am deeply indebted to my supervisor, Dr. W. Robert J. Funnell, not only for his guidance, but for his understanding and patience, and for allowing me to do some of my research and writing remotely.

I thank my dear colleague, Hanif M. Ladak, for answering my endless barrage of questions, no matter how trivial, especially when I was away from McGill.

I also thank my sister, Suchandra T. Ghosh, and my oldest and dearest friend, Debbie Harmady, for their constant moral support and encouragement. I also thank the rest of my friends, both at McGill and elsewhere, who helped me deal with my software problems while I worked remotely and gave me moral support.

## TABLE OF CONTENTS

<b>ABSTRACT</b>	<b>i</b>
<b>RÉSUMÉ</b>	<b>i</b>
<b>ACKNOWLEDGEMENTS</b>	<b>ii</b>
<b>TABLE OF CONTENTS</b>	<b>iii</b>
<b>LIST OF FIGURES</b>	<b>vi</b>
<b>CHAPTER 1. INTRODUCTION</b>	<b>1</b>
<b>CHAPTER 2. ANATOMY</b>	<b>3</b>
2.1 INTRODUCTION	3
2.2 EARDRUM	4
2.3 THE OSSICULAR CHAIN	5
2.3.1 Malleus	6
2.3.2 Incus	7
2.3.3 Stapes	8
2.3.4 Ossicular Joints	8
2.4 THE MIDDLE-EAR MUSCLES	10
2.5 CAT MIDDLE-EAR ANATOMY VS. HUMAN MIDDLE EAR ANATOMY	10
2.5.1 Middle-Ear Cavities and Eardrum	10
2.5.2 Ossicles	12
2.6 SUMMARY	13
<b>CHAPTER 3. MIDDLE-EAR MECHANICS AND MODELS</b>	<b>14</b>
3.1 INTRODUCTION	14
3.2 MIDDLE-EAR MECHANICS	14
3.2.1 TRANSFORMER PRINCIPLES	14
3.2.2 AXIS OF ROTATION AND STAPES FOOTPLATE MOTION	17
3.2.3 SUMMARY	18
3.3 MIDDLE-EAR MODELS	18
3.3.1 Introduction	18
3.3.2 Lumped-Parameter Models	18
3.3.3 Distributed-Parameter Models	19
3.3.4 Conclusion	21

<b>CHAPTER 4. THE FINITE-ELEMENT METHOD</b>	<b>22</b>
4.1 OVERVIEW	22
4.2 MESH SELECTION	23
4.3 FINITE-ELEMENT ANALYSIS WITH THIN-SHELL ELEMENTS	23
4.3.1 Introduction	23
4.3.2 Stresses and Strains in the Case of Plane Stress	24
4.3.3 Constitutive Equations	25
4.3.4 Solution Procedure	26
4.4 SUMMARY	27
<b>CHAPTER 5. DESCRIPTION OF MODEL</b>	<b>29</b>
5.1 EARDRUM	29
5.1.1 Material Properties	29
5.1.2 Geometry	29
5.2 OSSICLES	31
5.2.1 Material Properties	31
5.2.2 Loading and Geometry	32
5.3 ACOUSTIC STIMULUS	34
5.4 BANDWIDTH MINIMIZATION	34
5.5 RANGE OF VALIDITY AND MODEL LIMITATIONS	35
<b>CHAPTER 6. RESULTS AND DISCUSSION</b>	<b>36</b>
6.1 DISPLACEMENTS OF THE FOOTPLATE	36
6.1.1 Introduction	36
6.1.2 <i>X</i> Displacements	36
6.1.3 <i>Y</i> Displacements	38
6.1.4 <i>Z</i> Displacements	39
6.2 DISPLACEMENTS OF THE INCUDOSTAPEDIAL JOINT	41
6.2.1 Introduction	41
6.2.2 <i>X</i> and <i>Y</i> Displacements of Incus-Side Nodes	41
6.2.3 <i>Z</i> Displacements of Incus-Side Nodes	44
6.2.4 <i>X</i> and <i>Y</i> Displacements of Stapes-Side Nodes	45
6.2.5 <i>Z</i> Displacements of Stapes-Side Nodes	46
6.2.6 Joint Compression vs. Shear	48
6.2.7 Range of Validity	50
6.2.8 Assumption of Linearity	50
6.3 EARDRUM AND MANUBRIAL DISPLACEMENTS	50
6.3.1 Introduction	50
6.3.2 Maximum Drum and Manubrial Displacements	51
6.3.3 Vibration Patterns on the Eardrum	52
6.4 CONCLUSION	55

<b>CHAPTER 7. CONCLUSIONS AND FURTHER DEVELOPMENTS</b>	<b>56</b>
7.1 CONCLUSIONS	56
7.2 FURTHER DEVELOPMENTS AND CLINICAL APPLICATIONS	57
<b>REFERENCES</b>	<b>59</b>

## LIST OF FIGURES

2.1	The outer, middle and inner ears	4
2.2	The human eardrum	5
2.3	The human ossicles	6
2.4	The eardrum and ossicular chain	6
2.5	Front view of the tympanic membrane and malleus, showing the axis of rotation	7
2.6	The incudomalleolar joint (human)	9
2.7	The incudostapedial joint (human)	9
2.8	Cat and human middle-ear anatomy	11
2.9	Outlines of cat and human eardrums	12
2.10	Ossicles of cat and human	13
5.1	Finite-element model of the cat middle ear	30
6.1	Footplate in $x$ - $y$ plane with nodes	37
6.2	$X$ displacements of the footplate	38
6.3	$Y$ displacements of the footplate	39
6.4	$Z$ displacements of the footplate	40
6.5	Incus-side incudostapedial joint nodal $x$ displacements	42
6.6	Incus-side incudostapedial joint nodal $y$ displacements	43
6.7	Incus-side incudostapedial joint nodal $z$ displacements	44
6.8	Stapes-side incudostapedial joint nodal $x$ displacements	45
6.9	Stapes-side incudostapedial joint nodal $y$ displacements	46
6.10	Stapes-side incudostapedial joint nodal $z$ displacements	47

6.11 Incudostapedial joint nodal compression	48
6.12 <i>X</i> Shear of the incudostapedial joint	49
6.13 <i>Y</i> Shear of the incudostapedial joint	49
6.14 Eardrum and manubrial displacements	51
6.15 Eardrum vibration patterns (Y.M. = $2 \times 10^3$ )	52
6.16 Eardrum vibration patterns (Y.M. = $2 \times 10^6$ )	53
6.17 Eardrum vibration patterns (Y.M. = $2 \times 10^{13}$ )	54

## CHAPTER 1. INTRODUCTION

A considerable amount of research has been conducted in the field of auditory mechanics in the past few decades. Many quantitative models of the middle ear have been developed, including lumped-parameter models, analytical models, and finite-element models. The complex geometry and material properties of the middle ear make it very difficult to model. Finite-element models handle these types of complexities in a structure more readily than do the lumped-parameter and analytical models and are becoming the popular choice in these types of intricate modelling problems.

Potential clinical applications of this research are in tympanoplasty, ossicular prosthesis development, and impedance tympanometry. A good quantitative middle-ear model may be able to tell clinicians and researchers which features of the eardrum (e.g., shape, Young's modulus, and thickness) are most important in determining its behaviour. This type of information can be used to guide the choice of tympanic-membrane graft material. For example, a good model might show clinicians that it is important to replicate the inhomogeneities in the thickness as closely as possible, or that it is important to select a particular Young's modulus for the drum. In the case of total tympanic-membrane replacement, it is possible to say whether the shape must be replicated as faithfully as possible. Likewise, by obtaining similar information about the ossicles and modelling ossicular grafts, it is hoped that a good finite-element model of the middle ear will potentially aid in the development of prostheses to correct hearing loss due to ossicular discontinuity. A good model could also lead to the development of more noninvasive, quantitative methods of evaluating middle-ear function with impedance tympanometry and other procedures.

Most models are constructed with assumptions that sometimes limit the response of the model to stimuli. In many finite-element middle-ear models, the incudostapedial joint is taken to be rigid, but studies have shown that the incudostapedial joint is flexible. Thus, the objective of this research is to add an explicit representation of a flexible

incudostapedial joint to an existing model and compare the response of this model to its predecessor, which contained a rigid incudostapedial joint.

A good understanding of this finite-element model of the middle ear starts with knowledge of middle-ear anatomy, which is reviewed in Chapter 2, and middle-ear mechanics, which is discussed in Chapter 3. An introduction to the finite-element method and derivations relevant to the particular type of finite element used in modelling the joint are discussed in Chapter 4. The finite-element model of the middle ear will be introduced in Chapter 5. The simulation results and the behaviour of the model will be discussed in Chapter 6, followed by conclusions and directions for further research in Chapter 7.

## **CHAPTER 2. ANATOMY**

### **2.1 INTRODUCTION**

The human ear consists of three sections: the outer ear, the middle ear, and the inner ear. The outer ear consists of the pinna and the ear canal. The middle ear consists of the eardrum, ossicles, muscles, and ligaments. The inner ear consists of the cochlea and the semicircular canals. Incoming sound first travels through the ear canal of the outer ear to the eardrum or tympanic membrane of the middle ear. The middle ear essentially conducts sound from the outer ear to the inner ear by means of vibrations from the eardrum to the ossicles and then to the oval window. The oval window leads into the cochlea, where sound energy is transformed into electrical impulses to be processed by the brain.

The middle-ear is a small air-filled cavity (about 2 cm<sup>3</sup>) which is lined with mucous membrane and contains a linked ossicular chain. The middle ear forms the link between the outer ear, which is filled with air, and the inner ear, which is filled with liquid. The impedance mismatch which exists between the air-filled outer ear and the liquid-filled inner ear would cause a great loss of sound energy if the middle ear did not exist; the most important function of the middle ear is to perform an impedance-matching task. This will be discussed in the next chapter. This chapter will describe the anatomy of the middle ear and the following chapter will discuss the function of the middle ear. The human outer, middle, and inner ears are shown in Figure 2.1; only structures relevant to the discussion here are labelled. The structures of the human middle ear are discussed in the following sections.

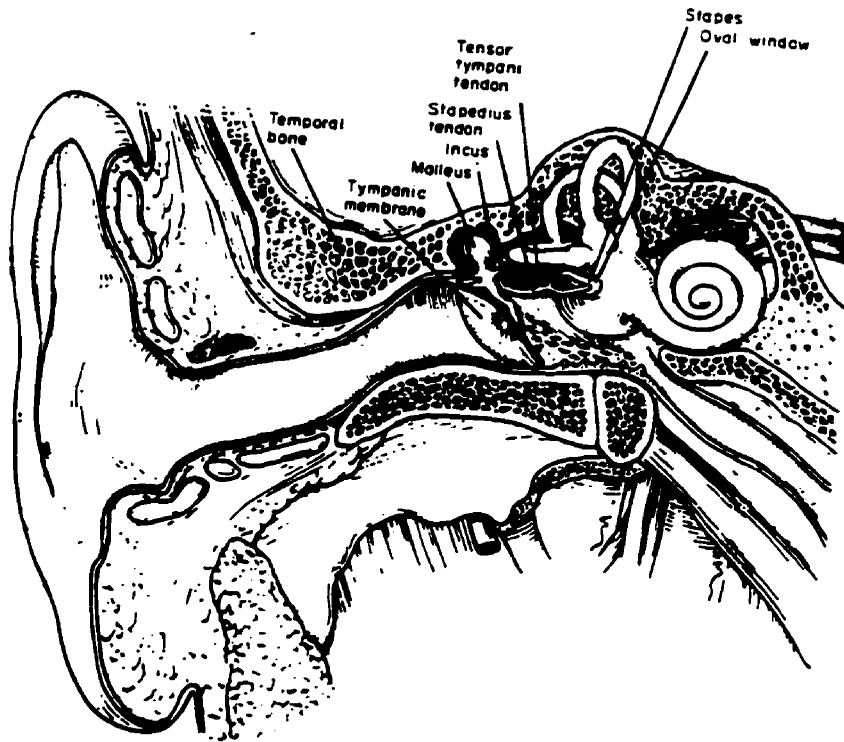


**Figure 2.1** The outer, middle, and inner ears (human). After Kessel and Kardon (1979).

## 2.2 EARDRUM

The shape of the eardrum or tympanic membrane in most mammals is somewhat round and conical. The apex points medially, and is convex outward. The deepest point in the cone, the apex, is called the umbo. The umbo marks the tip of the manubrium (see below).

Mammalian eardrums consist of the pars tensa and pars flaccida. The pars tensa is a very thin sheet of connective tissue; it ranges in thickness from 30-90  $\mu\text{m}$  in the human (Lim, 1970). It is a multi-layered tissue consisting of an outer epidermal layer, an inner mucosal layer, and the lamina propria. The outer epidermal layer is continuous with the

ear canal. It is similar to other skin in the body except for the absence of hair follicles and glands. Its outermost layer is the stratum corneum, which is a dense, thin material. The inner mucosal layer is a continuation of the mucous lining of the middle-ear cavity. Mechanically, the lamina propria is the most important part of the pars tensa. The outer radial fibres and the inner circular fibres are its main components. Both of these types of fibres are primarily collagenous. The radial fibres run from the manubrium to the annular ligament. The circular fibres start on one side of the manubrium, then circle around and below the umbo. They attach again on the other side of the manubrium. The pars flaccida is more elastic than the pars tensa and is located superior to it. The pars flaccida is similar to the pars tensa but has relatively few fibres. It ranges in thickness from 30  $\mu\text{m}$  to 230  $\mu\text{m}$  in the human (Lim, 1970). The human eardrum is shown in Figure 2.2.

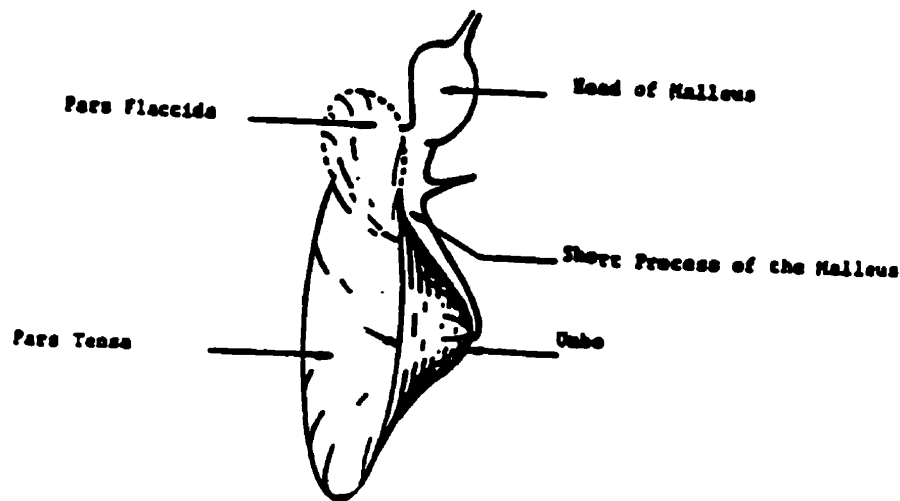


**Figure 2.2** The human eardrum. From Rabbitt (1985).

### 2.3 THE OSSICULAR CHAIN

The ossicular chain is suspended by ligaments and muscles and consists of the malleus, incus and stapes. The human ossicles are shown in Figure 2.3. Figure 2.4 shows the orientation of the human ossicular chain with respect to the eardrum.

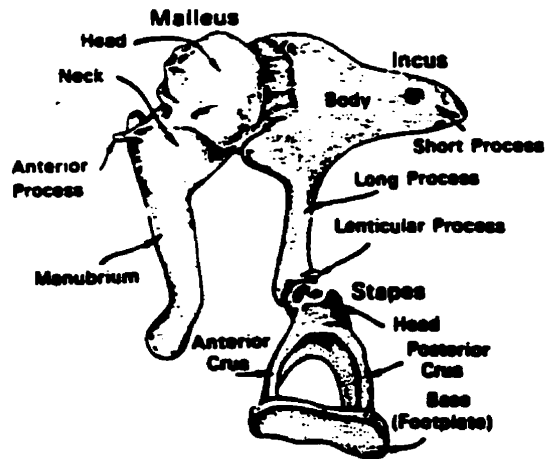


**Figure 2.3** The human ossicles. From Schuknecht and Gulya (1986), after Anson and Donaldson (1967).

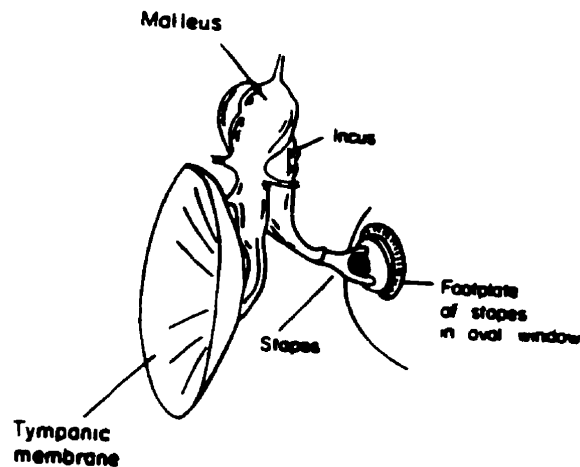


**Figure 2.4** The eardrum and ossicular chain. From Pickles (1988).

### 2.3.1 Malleus

The outermost ossicle is the malleus. The malleus is composed of the manubrium, head, neck, and lateral and anterior processes. The manubrium is firmly attached to the eardrum at the umbo and at the lateral process (in the human). The malleus is kept in place by one articulation or joint, the tensor tympani tendon and five ligaments: the anterior suspensory ligament, lateral suspensory ligament, superior suspensory ligament,

anterior malleal ligament, and posterior malleal ligament. According to Schuknecht and Gulya (1986), the anterior suspensory ligament lies superior to the anterior malleal ligament and suspends the head of the malleus in the tympanic cavity, as does the superior suspensory ligament; the lateral suspensory ligament suspends the neck of the malleus; the posterior malleal ligament is a thickening of a malleal fold; the anterior malleal ligament, together with the anterior process of the malleus, is in the ossicular axis of rotation, which is shown in Figure 2.5. Kobayashi (1955) found that some of these ligaments did not appear to be true ligaments in that histologically and/or macroscopically, their structure was not that of a ligament. In addition, the ligaments varied greatly across the 22 kinds of experimental animals that he studied, including the human.

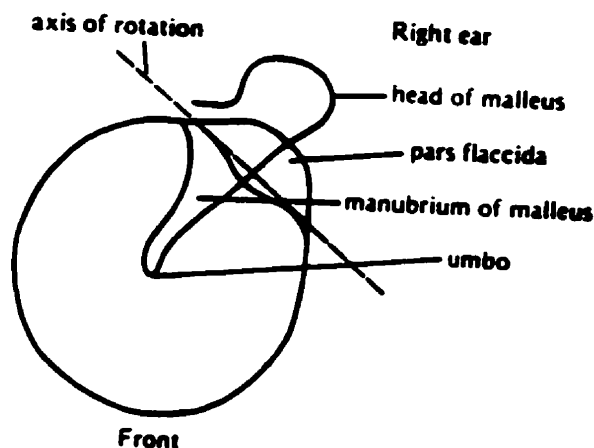


**Figure 2.5** Front view of the tympanic membrane and malleus, showing the axis of rotation. From Yost and Nielson (1985).

### 2.3.2 Incus

The incus is the largest of the auditory ossicles and consists of a body, a long process, and a short process. The incus is secured by three ligaments. The posterior incudal ligament holds the short process in the posterior incudal recess while the medial and lateral incudomalleal ligaments bind the body of the incus to the head of the malleus.

### 2.3.3 Stapes

The smallest link in the ossicular chain is the stapes, which is the innermost ossicle. The stapes consists of a base or footplate, two crura (legs), a neck, and a head. The footplate of the stapes is fixed by the annular ligament to the vestibular or oval window. The annular ligament is basically a ring of elastic fibres around the circumference of the footplate.

### 2.3.4 Ossicular Joints

The three ossicles are joined together by articulations or joints. The incudomalleolar joint connects the head of the malleus to the body of the incus and the incudostapedial joint connects the lenticular process of the incus with the head of the stapes. Gulya and Schuknecht (1986) define both joints as non-weight-bearing, synovial, diarthrodial articulations. They found that the articulating surfaces of the incudomalleolar joint are lined by cartilage, but the incudostapedial joint does not have interarticular cartilage. The incudomalleolar joint has a large saddle-shaped surface; the thickness of the joint is much smaller than the surface. The incudostapedial joint surface is very small compared to that of the incudomalleolar joint (incudostapedial joint dimensions are given in Chapter 5). Figure 2.6 shows the incudomalleolar joint and Figure 2.7 shows the incudostapedial joint (both are from the human).

The incudomalleolar joint is fairly rigid, i.e., the heads of the malleus and incus move more or less as one body. There is some experimental evidence that the incudostapedial joint is not rigid (Guinan and Peake, 1967). These studies show that the joint does translate at higher frequencies; the joint was found to compress while “slipping sideways” during condensation of the sound wave and stretch during rarefaction.

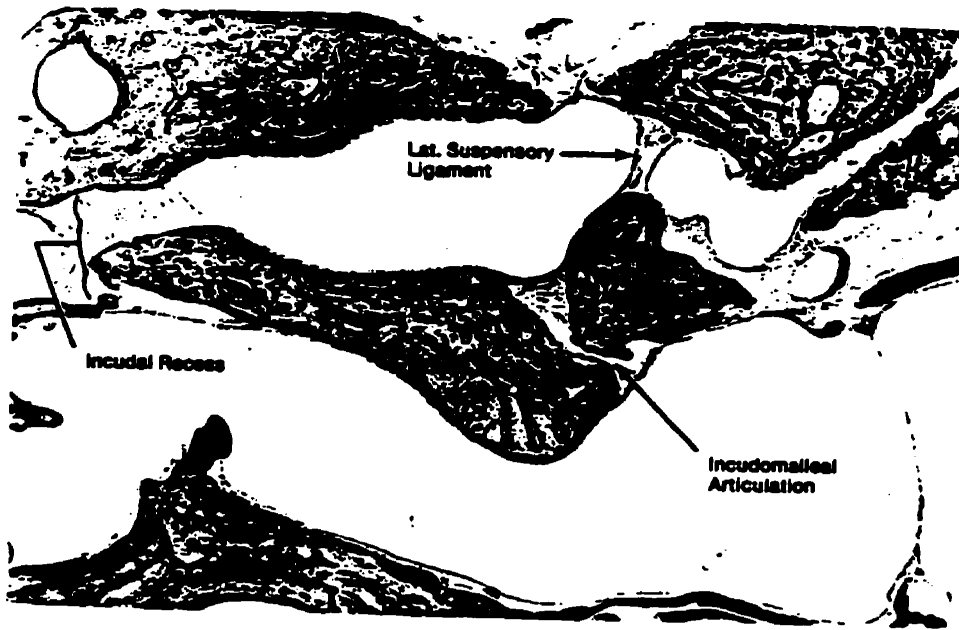


**Figure 2.6** The incudomalleal joint (human). From Gulya and Schuknecht (1986).



**Figure 2.7** The incudostapedial joint (human). From Gulya and Schuknecht (1986).

## 2.4 THE MIDDLE-EAR MUSCLES

There are two muscles in the middle ear, the stapedius muscle and the tensor tympani muscle. Both are striated muscles. The stapedius muscle is the smallest of all the skeletal muscles. Contraction of the stapedius muscle moves the anterior border of the footplate in a lateral direction and the posterior border in a medial direction. This causes the footplate of the stapes to tilt, which stretches the annular ligament and thereby stiffens the footplate, reducing its response to acoustic stimulation. The tensor tympani muscle moves the anterior border of the footplate laterally and pulls the umbo inward. Thus, the tensor tympani muscle acts with the stapedius muscle to modify the movements of the ossicles.

## 2.5 CAT MIDDLE-EAR ANATOMY VS. HUMAN MIDDLE-EAR ANATOMY

The anatomy of the cat middle ear is somewhat similar to the human middle ear. For example, the three ossicles in the cat middle ear resemble the human ossicles and the eardrum of the cat has the same basic shape as the human eardrum. The similarities and differences between the human middle ear and cat middle ear are discussed in the sections which follow.

### 2.5.1 Middle-Ear Cavities and Eardrum

Both the cat and human have an air-filled middle-ear cavity (tympanum). In the cat, the tympanum is larger and divided into two cavities, the ectotympanum (bulla) and the enyotympanum, which are separated by a bony septum. This septum contains an orifice which allows transmission of sound between the two cavities. In addition, the epitympanic recess or attic in the human is larger than that in the cat and there are no mastoid air cells in the cat. A schematic representation of that cat and human middle ears can be seen in Figure 2.8.

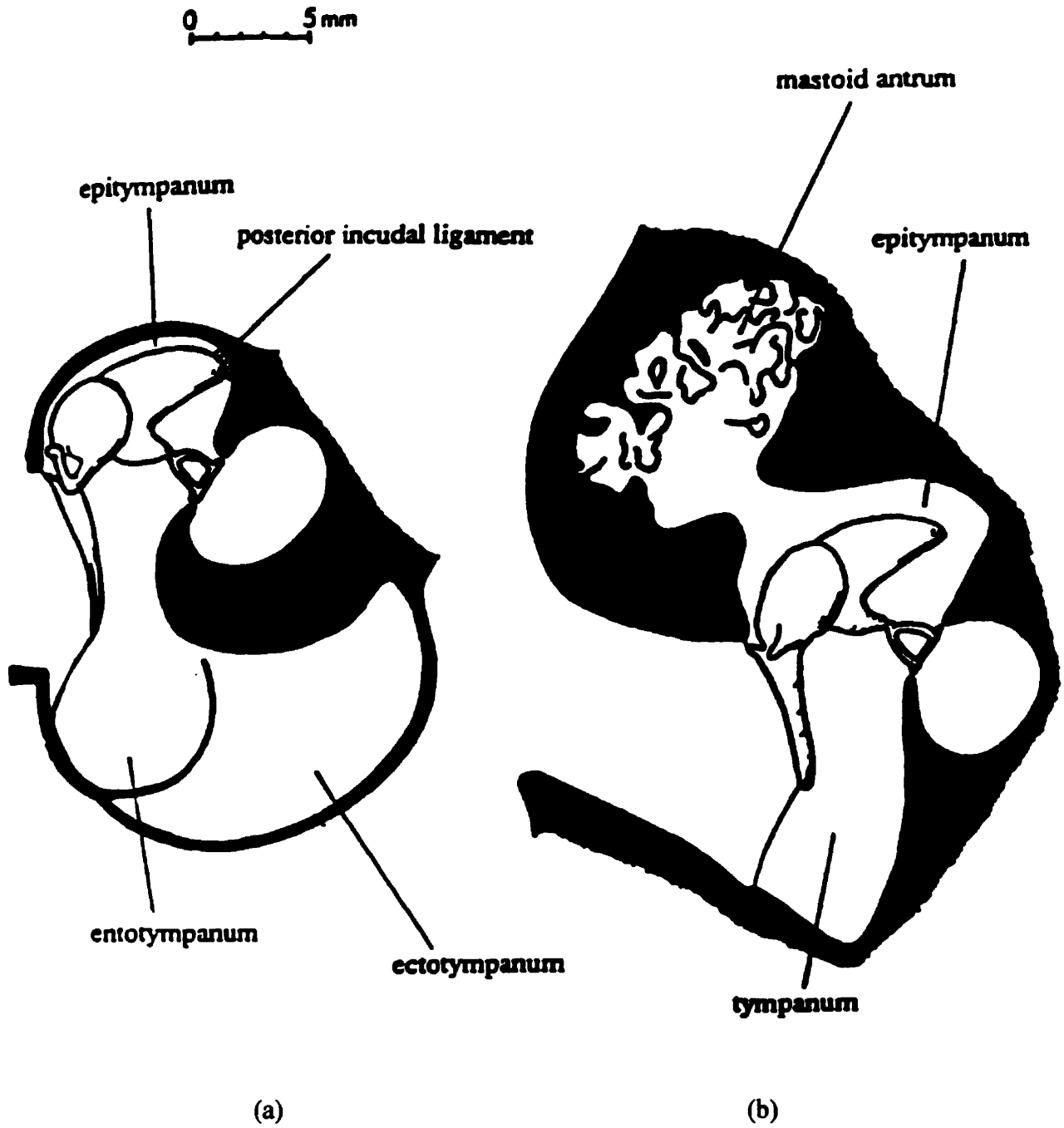


**Figure 2.8** (a) Cat and (b) human middle-ear anatomy. From Funnell (1989), after Funnell (1972).

The cat and human eardrum are both conical in shape and are convex outward. The human eardrum is roughly circular while the cat eardrum is somewhat elongated (Ladak, 1993). This is shown in Figure 2.9.

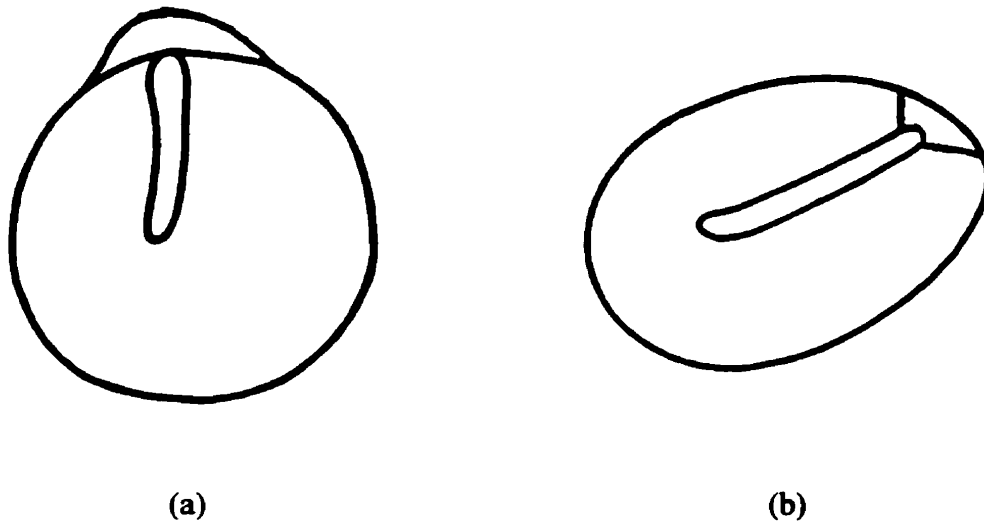


**Figure 2.9** Outlines of (a) cat and (b) human eardrums. From Funnell (1975), (a) after Fumigalli (1949), (b) after Khanna (1970).

### 2.5.2 Ossicles

As stated above, both the cat and human have an ossicular chain consisting of the malleus, incus and stapes. They are anatomically very similar; the differences are in the details of the ossicles. Although the configuration of the malleus and the incus are different in the cat ear, they are similar in that the incus and the malleus are suspended from the skull by ligaments (Funnell and Laszlo, 1978). As stated above, the manubrium is firmly attached to the eardrum at the umbo and at the lateral process in the human; in the cat, it is firmly attached along its whole length. In addition, according to Khanna (1970), the manubrium is nearly perpendicular to the ossicular axis of rotation in the human, while in the cat, this angle is roughly  $30^\circ$ . Finally, for the human, the position of the stapedial footplate is at the level of the umbo, while in the cat, the footplate is found

behind the upper end of the manubrium. The ossicles of the cat and human are shown in Figure 2.10.

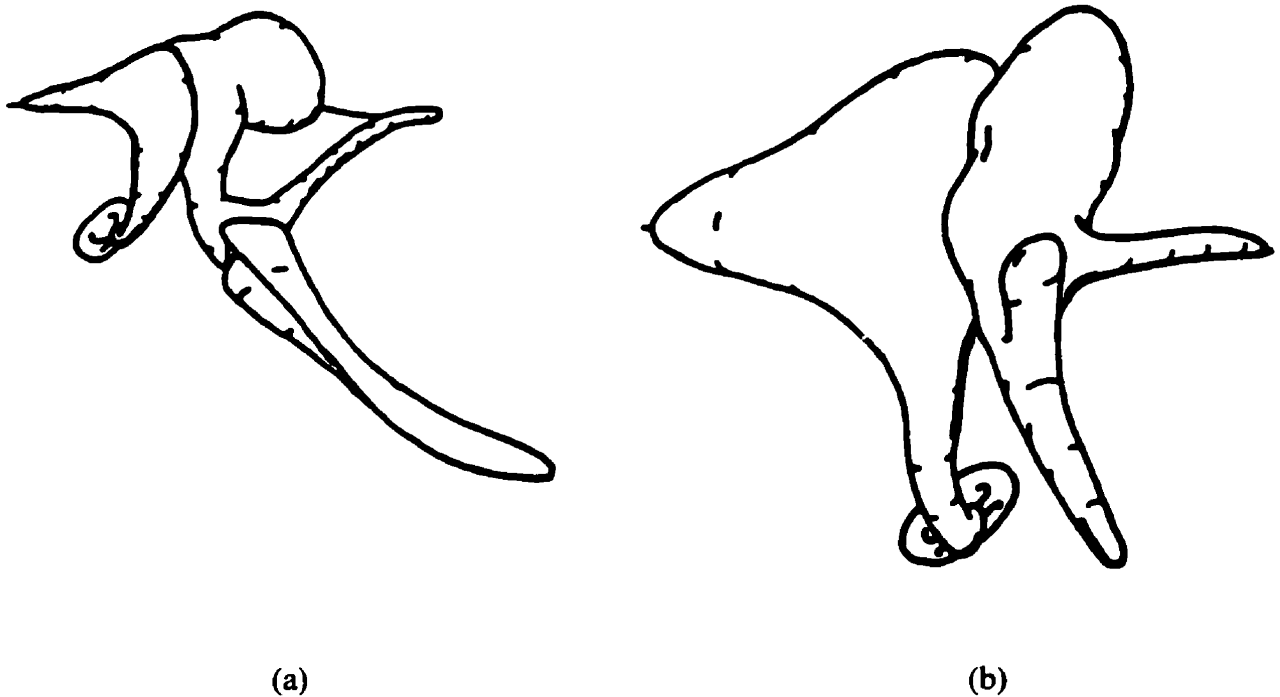


**Figure 2.10** Ossicles of (a) cat and (b) human (right ear, lateral view). From Funnell (1972), (a) after Jayne (1898), (b) after Nager and Nager (1953).

## 2.6 SUMMARY

In summary, the tympanic cavity or tympanum is an air-filled cavity which contains a chain of three linked bones or ossicles. These ossicles transmit the vibrations of the tympanic membrane to the inner ear. The ossicular chain is suspended in the middle-ear cavity by several ligaments and is acted upon by two muscles. The cat middle ear has been deemed similar enough to human middle ear to be used as a basis for the model of the middle ear. The function of the middle ear will be discussed in the following chapter.

## **CHAPTER 3. MIDDLE-EAR MECHANICS AND MODELS**

### **3.1 INTRODUCTION**

The primary function of the middle ear is that of an impedance transformer. As discussed in previous chapters, incoming sound waves travel through an air-filled space and hit the eardrum. This causes the eardrum to vibrate. The eardrum is connected to the ossicles which start to vibrate when the eardrum is set in motion. The vibrations travel via the ossicles in the air-filled middle-ear cavity to the oval window, which leads to the liquid-filled cochlea. The liquid in the cochlea is much denser than air, and therefore has a greater acoustical impedance than air. When sound waves travel from a less dense medium to a denser medium, much of the sound energy is reflected. The middle ear acts as an impedance transformer by reducing the reflection of the waves, but it is not clear exactly how the transformer ratio is effected.

### **3.2 MIDDLE-EAR MECHANICS**

#### **3.2.1 Transformer Principles**

The middle ear acts as a transformer by using three principles. First, the surface area of the oval window is smaller than that of the tympanic membrane. Therefore, the sound wave pressure is concentrated on a smaller area. This increases the pressure of the sound waves at the oval window. The pressure is increased in proportion to the ratio of the two areas. According to Bess and Humes (1995), the eardrum area which is directly involved in forming a link between the outer and middle ears (the effective area) is about  $55 \text{ mm}^2$ . The effective area of the stapes footplate is approximately  $3.2 \text{ mm}^2$ . Since the force being applied at the eardrum is about the same force that is reaching the footplate, the pressure at the footplate must be greater than that at the eardrum. This can be shown by the following formula:

$$p = \frac{F}{A} \quad (3.1)$$

where  $p$  is the pressure,  $F$  is the force and  $A$  is the area.  $F$  is the same for both the eardrum and footplate, so the pressure at the footplate is  $F/3.2$  and the pressure at the eardrum is  $F/55$ . This means that the pressure at the oval window is about 17 times that at the eardrum, which greatly reduces the reflection of the sound waves.

Second, the lever action of the ossicles, caused by the fact that the long process of the incus is shorter than that of the manubrium, increases the force of the incoming sound waves while decreasing the velocity at the stapes footplate. Sound pressure applies a force on the tympanic membrane and is transferred to the cochlea at the footplate of the stapes through the rotation of a lever mechanism. The lengths of the lever arms are the distances from the axis of rotation to (1) the head of the stapes; and (2) a point on the manubrium which represents the effective centre of action of the incoming sound pressure.

The lever mechanism and area ratio has been described in great detail by Relkin (1988). According to Relkin, the “impedance transformer” action of the middle ear is shown in the following equation:

$$\frac{Z_e}{Z_f} = \left( \frac{A_f}{A_e} \right)^2 \left( \frac{l_i}{l_m} \right)^2 \quad (3.2)$$

where  $Z_e$  is the impedance at the eardrum,  $Z_f$  is the impedance at the footplate,  $A_f$  is the area of the footplate,  $A_e$  is the area of the eardrum,  $l_i$  is the length of the lenticular process of the incus, and  $l_m$  is the length of the manubrium. There is a range of plausible values for  $l_i/l_m$ , from .77 (Yost and Nielsen, 1986) to .50 (Guinan and Peake, 1967), but this lever-arm ratio is always smaller than one. Hence, the lenticular process is shorter than the manubrium and the area of the footplate is less than the area of the eardrum, causing

the right side of Equation 3.2 to be less than one. Therefore, for Equation 3.2 to hold true, the impedance at the tympanic membrane is reduced relative to the impedance at the footplate. According to Relkin, “the acoustic impedance of the fluid of the cochlea at the oval window is decreased at the tympanic membrane to a value that is closer to the impedance of air”. This means that the amount of incoming sound energy that will be transmitted by the middle ear to the cochlea is increased.

Note that these analyses of the transformer action of the middle ear are very much oversimplified because they ignore the distributed nature of the structures and forces involved and also ignore the true modes of vibration of both the eardrum and the ossicles. The eardrum does not vibrate like a hinged plate and at most frequencies the ossicles do not rotate about a fixed axis of rotation.

The third mechanism of the middle-ear transformer is that the curvature of the eardrum amplifies the pressure of the sound wave before it is applied to the manubrium (Tonndorf and Khanna, 1970). This hypothesis was originally proposed by Helmholtz (1869) and is known as the curved-membrane effect. Helmholtz stated that a sound striking the eardrum surface will be amplified because of the slight curvature of the fibres and because of the fibre arrangement. The middle section of the radial fibres is fairly free to move. The amplitude of the radial fibre is greater in the centre, although it is less forceful. At the umbo, it is reduced in amplitude but increased in force. Thus the umbo, and therefore the ossicles, show vibrations which are smaller in amplitude and stronger in force than the sound waves or air particles which hit the surface of the eardrum. In a recent study, Funnell (1996) found that “certain regions of the eardrum are more effective in driving the manubrium than can be explained on the basis of their distance from the axis of rotation”. This phenomenon was found to depend on the curvature of the eardrum, but does not require tension or anisotropy as Helmholtz proposed.

### 3.2.2 Axis of Rotation and Stapes Footplate Motion

The movements of the ossicular chain vary with the frequency and intensity of incoming sound waves. The mass of the ossicles is distributed around an axis of rotation running from the anterior malleolar ligament to the posterior incudal ligament. However, it has been found that the position of the axis changes with frequency (e.g., Decraemer *et al.*, 1991) and probably depends more on the characteristics of the middle-ear ligaments than on the mass distribution (Yost and Nielsen, 1985) and perhaps even more so on the characteristics of the eardrum.

Dissimilar types of stapes footplate motion have been observed by different researchers, possibly due to differences in experimental techniques and experimental conditions. Some studies indicate that when the sound intensity is moderate, the ossicular chain is set in motion in a way that causes the posterior portion of the footplate of the stapes to swing about an imaginary axis drawn vertically through the posterior crus while the anterior portion of the footplate pushes in and out of the cochlea (Kobrak, 1959; Békésy, 1960). This action may be due to the asymmetric length of the annular-ligament fibres. This movement of the footplate is thought to change dramatically at very low frequencies (<100 Hz) and at frequencies greater than 1.2 kHz. At the low frequencies, the axis of rotation is through the crura, perpendicular to the previous vertical axis; stapes motion becomes similar to that of a seesaw, rocking about its longitudinal axis (Gyo *et al.*, 1987). When the intensity of the sound wave is high and the frequency is greater than 1.2 kHz, Gyo *et al.* (1987) found that both types of footplate rotations occur simultaneously. Thus, due to this complex form of rotation, little motion of the cochlear fluids is observed when the intensity is increased even further. Other researchers (Guinan and Peake, 1967; Dankbaar, 1970; Gunderson, 1972; Vlaming and Feenstra, 1986) have found that the footplate exhibits piston-like motion, moving in and out of the oval window.

### 3.2.3 Summary

In summation, the middle ear couples sound energy from the outer ear to the cochlea. The outer ear is air-filled and the cochlea is filled with liquid, which causes an impedance mismatch. This impedance mismatch would cause much of the sound entering the ear to be reflected and the auditory system would lose much of its sensitivity. The middle ear helps to match the impedance of the outer ear to the much higher impedance of the cochlear liquid. The axis of rotation of the ossicles changes as the intensity and frequency of incoming sound waves change.

## 3.3 MIDDLE-EAR MODELS

### 3.3.1 Introduction

Many mathematical models have been constructed over the past few decades to model the mechanical behaviour of the middle ear. They may be divided into lumped-parameter and distributed-parameter models.

### 3.3.2 Lumped-Parameter Models

Lumped-parameter models (e.g., Zwislocki, 1962; Shaw and Stinson, 1986; Vlaming, 1987) are usually cast in the form of mechano-optical circuits, or equivalent electrical circuits. In these models, the mechanical or acoustical behaviour of a relatively large anatomical structure or a group of structures is represented by a combination of three idealized circuit elements: a point mass, an ideal spring and an ideal damper. The corresponding parameters are usually determined empirically, i.e., the behaviour of all or part of the model is fit to experimental results as closely as possible. A major drawback of lumped-parameter models lies in the fact that the model parameters are often not closely tied to physiological or anatomical data. For example, a mass parameter which models rotating structures actually represents a moment of inertia and thus depends on the

position and orientation of the axis of rotation. Such models are applicable only at fairly low frequencies.

### 3.3.3 Distributed-Parameter Models

A distributed-parameter model, in contrast, is defined in terms of anatomical shape parameters and biomechanical properties, independent of the nature of the mechanical behaviour. Distributed-parameter modelling may be done analytically (Esser, 1947; Gran, 1968) or semi-analytically (Rabbitt and Holmes, 1988), but quickly becomes unmanageable for complicated systems. Finite-element models are numerical distributed-parameter models.

Esser (1947) and Gran (1968) have provided analytical models of the eardrum. The eardrum was modelled as a circular membrane under tension by Esser. The drum was clamped along its circumference and the malleus was represented as a force applied to a point at the centre of the drum. This analysis resulted in several multiple integrals, some of which could only be solved if the curvature of the eardrum was ignored. Funnell and Laszlo (1978) established, however, that the curvature is very important to eardrum function. The eardrum was modelled as a plane circular plate with the manubrium positioned radially by Gran (1968). This system was very mathematically complex even though this model was oversimplified (Funnell, 1975).

A fibre-composite shell model of the eardrum (semi-analytical) has been constructed by Rabbitt and Holmes (1986). They derived equations to describe structural damping, transverse inertia and membrane-restoring forces. Geometric and material assumptions were made to obtain a closed-form asymptotic solution. The problem with this model was that each assumption affected subsequent problem formulation, which makes it difficult to change them.

The finite-element method is the most powerful and general approach to distributed-parameter modelling. The finite-element method handles complex structures by breaking up the complex structures into simple elements. Although the finite-element method is computationally demanding, it has relatively few free parameters whose values need to be adjusted to fit data. According to Funnell (1975), most of the parameters needed in his finite-element models of the middle ear have a very direct relationship to the structure and function of the system, and can be estimated independently of the experimental situation being modelled. This type of model can easily simulate behaviour changes that occur at high frequencies.

Funnell (1975) first used the finite-element method to analyze the structure and function of the eardrum. Subsequently, Funnell and Laszlo (1978) modelled the cat eardrum as a three-dimensional thin shell. This model was valid for low frequencies (less than 1-2 kHz) and for physiological sound levels. This model indicated that the most important factors affecting the low-frequency behaviour of their finite-element model were the curvature and conical shape of the eardrum as well as its anisotropic material properties. The stiffness and thickness of the pars tensa were found to be important as well. The characteristics which were found to be less important were boundary conditions, Poisson's ratio (the ratio of the lateral strain to the longitudinal strain), ossicular loading, and air loading.

Funnell (1983) expanded this model to include inertial effects, and calculated the natural frequency and mode shapes. These agreed fairly well with experimental results obtained by Khanna and Tonndorf (1972). The results obtained from this model indicated that the frequency range of the eardrum is extended by its conical shape and curvature. Ossicular parameters did not appear to have much effect on the natural frequencies and mode shapes of the eardrum. This model was further expanded by Funnell *et al.* (1987) to calculate the damped frequency response. They used a range of values because the experimental data needed to estimate the damping effects are scarce, especially at high frequencies. The frequency response of the eardrum away from the manubrium showed

sharp variations in this model. The variations were smoother for points on the manubrium. This was even true when there was no ossicular loading which seemed to indicate that spatial integration over the eardrum occurred at the manubrium, which is consistent with the work of Decraemer *et al.* (1987). Further improvements in the model were made by Funnell *et al.* (1992), and they found that the manubrium bends and twists at frequencies above a few kHz and maybe even at frequencies as low as 1 - 2 kHz. Finite-element middle-ear models have also been developed recently by other groups (e.g., Wada *et al.*, 1992; Williams and Lesser, 1990).

#### 3.3.4 Conclusion

Lumped-parameter and distributed-parameter models (including finite-element models) have been developed to model the mechanical behaviour of the middle ear. However, the complex material properties and irregular geometry of the various structures of the middle ear make it difficult to develop accurate quantitative models. The limitations of the various models were discussed and it was concluded that the finite-element method can handle these modelling problems fairly well and some existing finite-element models show consistency with experimental data.

## **CHAPTER 4. THE FINITE-ELEMENT METHOD**

### **4.1 OVERVIEW**

The finite-element method can be used to solve problems in structural analysis to determine stresses, strains, and displacements in a structure. In the finite-element method, the complex structure to be analyzed is divided into small, simply-shaped regions, or elements. This is known as mesh generation. These elements are connected at points called nodes. The larger the number of nodes per element, the more sophisticated the element. The finite-element method can make a structure easier to model since the governing equations within each element are defined by functions which are much simpler than those required for the entire structure.

The finite-element method is implemented in the following manner. First, the structure to be analyzed is divided into elements, which are subject to the following constraint: the elements must have identical common nodal displacements at a common node. The desired field is then represented by functions defined over each element. Then the mechanical response of each element to the applied load is analyzed; in this process, a stiffness matrix and load vector is obtained for each element in the structure. The stiffness matrix contains the coefficients of the equilibrium equations which are determined from the geometric and material properties of an element by using energy or variational principles. The detailed mechanical analysis of an element type is completed just once; then the matrices for individual elements are calculated using the individual element coordinates and properties in a canned formulation for that element type. After stiffness matrices and load vectors have been obtained for all of the elements, they are combined into a structure matrix equation. In this equation, nodal displacements in the structure are related to nodal loads. Then, the boundary conditions are applied and the unknown nodal displacements can be obtained from the solution of the structure matrix equation.

## 4.2 MESH SELECTION

As discussed in the previous section, mesh generation is the process of dividing a structure into elements. Some researchers believe that it is often best to use the simplest elements possible; the simpler the element, the simpler the calculations within the element. Other researchers prefer to use higher-order elements, which can be used in smaller numbers. After the element type is selected, the material properties of the element, such as material type, Young's modulus, and Poisson's ratio must be chosen.

The next step is to decide how many elements should represent the structure. Generally, the finer the mesh, the more accurate the solution in the entire structure. Unfortunately, the greater the number of elements in the structure, the greater the amount of time needed to solve all the equations in the system. Thus, a very fine mesh is computationally very taxing. A very coarse mesh would take comparatively little computational time, but the displacements of the model would not be as accurate; thus it is important to find a good mesh resolution for the model. Usually, the best way to find a suitable mesh resolution is to find the coarsest mesh for which the displacements are close enough to the true values. Thus, a coarse mesh should be used first and the displacements should be recorded; then, the mesh resolution should be increased and the displacements should be compared to the previous results. The mesh resolution should be continually increased until the results converge. The mesh that is selected for the model should be the coarsest mesh for which the results begin to converge or for which the results are good enough for the particular purpose at hand.

## 4.3 FINITE-ELEMENT ANALYSIS WITH THIN-SHELL ELEMENTS

### 4.3.1 Introduction

Most of the elements used in this model (except for the boundary elements) are two-dimensional triangular thin-shell elements. As discussed in Chapter 5, the

incudostapedial joint is also modelled by these elements, which are thin plates characterized by very small dimensions in the  $z$  direction (thickness). The shell elements used in this model have bending stiffness and can be loaded with out-of-plane forces. They have three nodes and six degrees of freedom at each node. The steps and equations used in the finite-element method will be outlined specifically in this section for the triangular thin-shell plane-stress elements as a simple introduction to finite-element analysis.

#### 4.3.2 Stresses and Strains in the Case of Plane Stress

The stress in an elemental volume of a loaded body may be defined in terms of the stress in that body by:

$$\{\sigma\}^T = [\sigma_x \ \sigma_y \ \sigma_z \ \tau_{xy} \ \tau_{yz} \ \tau_{zx}] \quad (4.1)$$

where  $\sigma_x$ ,  $\sigma_y$ , and  $\sigma_z$  are the normal components of stress and  $\tau_{xy}$ ,  $\tau_{yz}$ , and  $\tau_{zx}$  are the shear components of stress. Similarly, the strain can be defined as

$$\{\epsilon\}^T = [\epsilon_x \ \epsilon_y \ \epsilon_z \ \gamma_{xy} \ \gamma_{yz} \ \gamma_{zx}] \quad (4.2)$$

where  $\epsilon_x$ ,  $\epsilon_y$ , and  $\epsilon_z$  are the normal components of strain and  $\gamma_{xy}$ ,  $\gamma_{yz}$ , and  $\gamma_{zx}$  are the shear components of strain. In the case of plane stress, the  $z$  components of stress and strain vanish. Thus, Equation 4.1 becomes

$$\{\sigma\}^T = [\sigma_x \ \sigma_y \ \tau_{xy}] \quad (4.3)$$

and Equation 4.2 becomes

$$\{\boldsymbol{\varepsilon}\}^T = [\boldsymbol{\varepsilon}_x \ \boldsymbol{\varepsilon}_y \ \boldsymbol{\gamma}_{xy}] \quad (4.4).$$

The formulas for the stress and strain components can be found in any solid mechanics text or any text on elasticity.

### 4.3.3 Constitutive Equations

Stresses and strains in a body are related by the generalized form of Hooke's law; for plane stress conditions, this is given by

$$\begin{Bmatrix} \boldsymbol{\sigma}_x \\ \boldsymbol{\sigma}_y \\ \boldsymbol{\tau}_{xy} \end{Bmatrix} = \begin{bmatrix} C_{11} & C_{12} & C_{13} \\ C_{21} & C_{22} & C_{23} \\ C_{31} & C_{32} & C_{33} \end{bmatrix} \begin{Bmatrix} \boldsymbol{\varepsilon}_x \\ \boldsymbol{\varepsilon}_y \\ \boldsymbol{\varepsilon}_{xy} \end{Bmatrix} \quad (4.5)$$

or

$$\{\boldsymbol{\sigma}\} = [\mathbf{C}]\{\boldsymbol{\varepsilon}\}^1 \quad (4.6)$$

where the  $C_{ij}$ 's are the material constants (defined below),  $\{\boldsymbol{\sigma}\}$  is the stress vector and  $\{\boldsymbol{\varepsilon}\}$  is the strain vector.

For an elastic, isotropic material in the case of plane stress, Equation 4.5 becomes

$$\begin{Bmatrix} \boldsymbol{\sigma}_x \\ \boldsymbol{\sigma}_y \\ \boldsymbol{\tau}_{xy} \end{Bmatrix} = \frac{E}{1-\nu^2} \begin{bmatrix} 1 & \nu & 0 \\ \nu & 1 & 0 \\ 0 & 0 & (1-\nu)/2 \end{bmatrix} \begin{Bmatrix} \boldsymbol{\varepsilon}_x \\ \boldsymbol{\varepsilon}_y \\ \boldsymbol{\varepsilon}_{xy} \end{Bmatrix} \quad (4.7)$$

<sup>1</sup> The notation used for matrices and vectors in this chapter is

Rectangular matrix: bold letter in square brackets, e.g.,  $[\mathbf{X}]$

Column matrix (vector): bold letter in curly brackets, e.g.,  $\{\mathbf{X}\}$

Row matrix (vector): bold letter in curly brackets with superscript T, indicating transpose, e.g.,  $\{\mathbf{X}\}^T$ .

where  $E$  is Young's modulus and  $\nu$  is Poisson's ratio.

#### 4.3.4 Solution Procedure

The solution procedure shown here is described in many finite-element texts; thorough descriptions can be found in: Desai and Abel, 1972; Norrie and de Vries; 1973; Cook *et al.*, 1989; Ross, 1985; and Yang, 1986. As discussed earlier, the first step in the finite-element solution procedure is to select the types of elements to be used to model the structure of interest and the mesh resolution. Once this step has been completed, the mechanical response of each element to the applied load is analyzed; in this process, a stiffness matrix and load vector is obtained for each element in the structure. The stiffness matrix relates the displacements at nodal points (the nodal displacements) to the applied forces at nodal points (the nodal forces). If  $\{\mathbf{F}\}$  is the vector of the nodal forces,  $\{\mathbf{q}\}$  is the vector of the nodal displacements, and  $[\mathbf{k}]$  is the stiffness matrix, then

$$\{\mathbf{F}\} = [\mathbf{k}]\{\mathbf{q}\} \quad (4.8)$$

The element stiffness matrix  $[\mathbf{k}]$ , for the triangular elements with six degrees of freedom used here, is derived by using the principle of minimum potential energy<sup>2</sup>; this states that in order to satisfy the equations of elasticity and equilibrium, the change of potential with respect to the displacement must be stationary.

$$[\mathbf{k}] = \iint [\mathbf{B}]^T [\mathbf{C}] [\mathbf{B}] t \, dx \, dy \quad (4.9),$$

where  $t$  is the thickness of the element and  $[\mathbf{B}]$  is the strain-displacement matrix.  $[\mathbf{B}]$  contains constants based on the  $x$  and  $y$  coordinates of the three nodes. Since the  $[\mathbf{C}]$  and  $t$  are constant here as well,

---

<sup>2</sup> A through derivation of equation 4.9 using the principle of minimum potential energy can be found in Yang (1986) and Desai and Abel (1972).

$$[\mathbf{k}] = At[\mathbf{B}]^T[\mathbf{C}][\mathbf{B}] \quad (4.10)$$

where  $A$  is the area of the triangular element.

The next step is to assemble the global or system stiffness matrix from the element stiffness matrices and the global force or load vector from the element nodal force vectors. The first step can be completed by using Equation (4.9) and systematically adding all of the element stiffnesses.

For the entire system,

$$\{\mathbf{P}\} = [\mathbf{K}]\{\mathbf{Q}\}, \quad (4.11)$$

where  $\{\mathbf{P}\}$  is the vector of nodal point loads (total load vector),  $[\mathbf{K}]$  is the system stiffness matrix, and  $\{\mathbf{Q}\}$  is the vector of nodal point displacements (nodal displacement vector for the entire body).  $[\mathbf{K}]$  can be found by systematically adding all of the stiffnesses of all elements in the system. This equation can be solved to obtain the unknown displacements in the body.

#### 4.4 SUMMARY

In the finite-element method, the region to be analyzed is divided into small subregions or elements so that the solution within each element can be represented by a function very much simpler than that required for the entire structure. These functions are chosen to ensure continuity of the solution throughout the continuum. The advantage of the finite-element method is that it has the ability to represent highly irregular structures such as those found in the middle ear.

The finite-element method has gained popularity in the past decade and is used in many disciplines. Accordingly, an increasing amount of finite-element software is becoming commercially available, which makes it more convenient to model complicated structures by the finite-element method. The finite-element software used here was SAP IV (Bathe *et al.*, 1973).

## CHAPTER 5. DESCRIPTION OF MODEL

### 5.1 EARDRUM

#### 5.1.1 Material Properties

The finite-element model of the middle ear is shown in Figure 5.1. The eardrum in this model is equivalent to previous models from this laboratory (Funnell, 1983; Funnell *et al.*, 1987); it is modelled as a homogeneous, isotropic, linearly elastic thin shell. Triangular elements constitute the thin shell mesh, which has a 'nominal resolution' of 15 elements/diameter (Funnell, 1983). In this model, the pars tensa has a Young's Modulus of  $2 \times 10^7$  Pa, an overall thickness (including the epidermal, fibrous, and mucosal layers) of  $40 \mu\text{m}$  and a Poisson's ratio of 0.3. The pars flaccida has a much lower stiffness than the pars tensa and consequently does not have much effect on the overall behaviour of the drum. At the time this model was constructed, it was thought that there was a section of the annular ligament which divides the pars tensa from the pars flaccida. Although it is now known that there is no such ligament (Funnell and Decraemer, 1996), it is still included in this model and has a thickness of  $300 \mu\text{m}$ . The remaining material parameters (Young's modulus and Poisson's ratio) are the same as those of the pars tensa. A high Young's modulus is assigned to the manubrium to make it essentially rigid, since it is actually part of the ossicular chain.

#### 5.1.2 Geometry

The eardrum has a conical shape, and the overall degree of curvature is represented by a dimensionless constant  $c$ . For any particular radial fibre  $f$ , this constant is found from the following equation:  $r_f = cd_f$ , where  $r_f$  is the radius of the fibre and  $d_f$  is the straight-line distance between the ends of the fibre (Funnell and Laszlo, 1978; Funnell, 1983). Funnell (1983) calculated the value of  $c$  by considering each node within the region corresponding

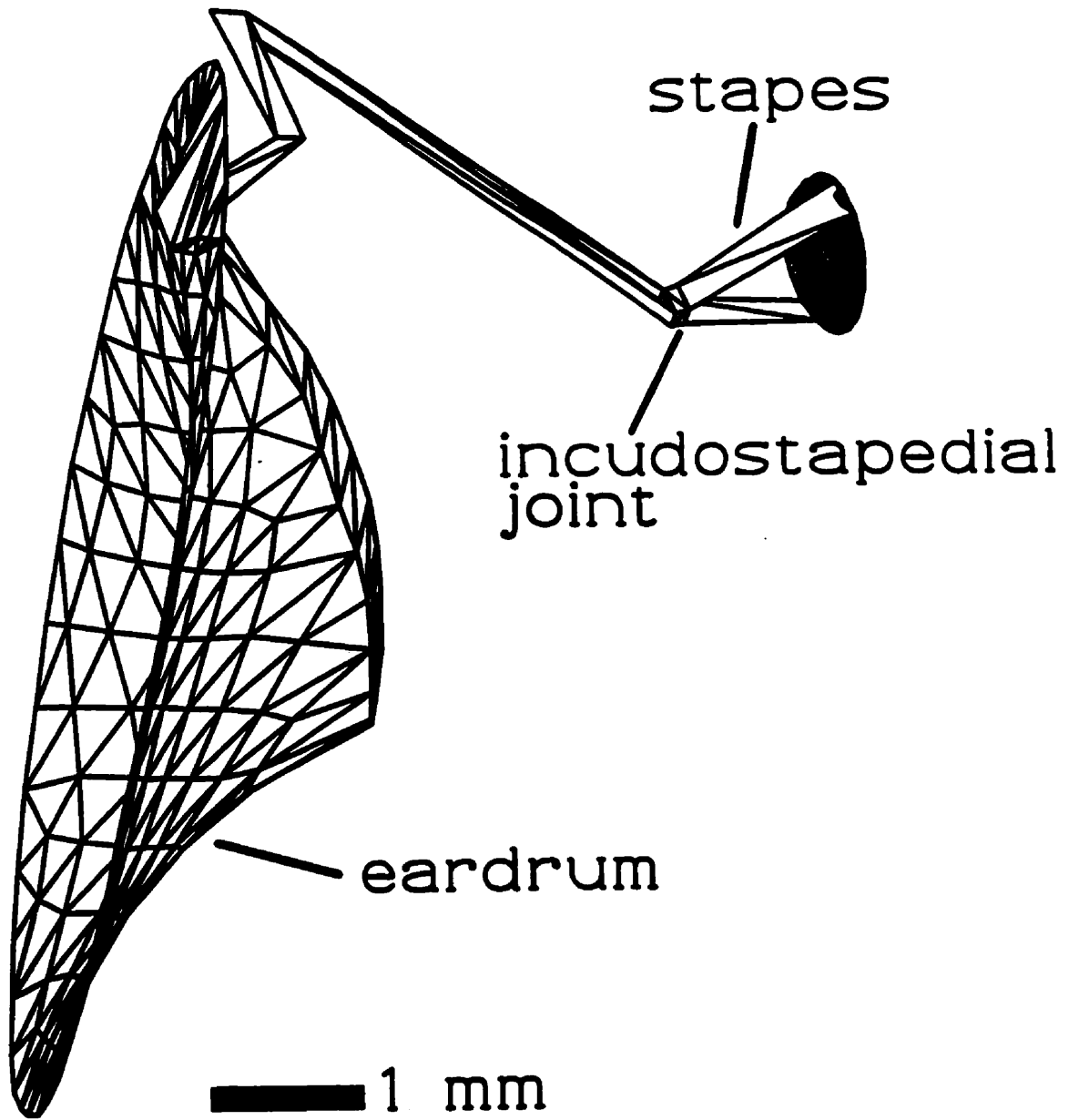


**Figure 5.1** Finite-element model of the cat middle ear.

to the pars tensa to be on a circular arc lying on a plane perpendicular to the plane of the tympanic ring, with one end on the manubrium and the other along the tympanic ring. In this model, the value of  $c$  was set to 1.19, because it was the smallest value that did not result in any nodes of the model lying above the plane of the tympanic ring.

## 5.2 OSSICLES

### 5.2.1 Material Properties

The ossicles are represented as homogeneous, isotropic bones with a Young's modulus of  $2 \times 10^{10}$  Pa and a Poisson's ratio of 0.3. The large thickness and high Young's modulus of the ossicles in the model (except for the footplate of the stapes and the incudostapedial joint) render them functionally rigid.

The head and neck of the malleus are modelled by five elements which link the manubrium rigidly to the fixed ossicular axis of rotation. Although this model has a fixed axis of incudomalleolar rotation, this is not realistic since the axis of rotation is not fixed (Funnell, 1996), as discussed in Chapter 3. The axis of rotation is connected rigidly to the incudostapedial joint by four elements which represent the long process of the incus. Each of the crura is depicted by two plate elements. In this model, the shapes of the elements which characterize the malleus, incus and stapedial crura are not significant since they are effectively rigid as a result of their thickness. In addition, the frequencies investigated in this model are sufficiently low for inertial effects to be absent.

The incudomalleolar joint is rigid in this model. The incudostapedial joint is modelled by 12 shell elements, forming a hollow box with eight nodes; the walls are shell elements representing the joint capsule with the Young's modulus varying from  $2 \times 10^2$  Pa to  $2 \times 10^{14}$  Pa and a Poisson's ratio of 0.3. The Young's modulus of the joint lies somewhere in the above range, and because there is little experimental evidence on which to base an estimate and the geometry of the joint is very crude, the Young's modulus is varied in

order to explore its effects on the behaviour of the model. The shell elements have a thickness of 0.0015 cm, and the size of the joint space between the incus and the stapes is 0.0035 cm, which is the  $z$  dimension. The  $x$  dimension is 0.0300 cm and the  $y$  dimension is 0.0552 cm. The dimensions are based on examination of serial histological sections of a cat middle ear.

The stapedial footplate is modelled by a mesh of triangular thin shell elements with a nominal resolution of 15 elements/diameter (Ladak and Funnell, 1993, Ladak and Funnell, 1996). The elements of the footplate mesh are smaller than the elements of the eardrum mesh because the diameter of the footplate is smaller than that of the eardrum. Ladak and Funnell (1996) obtained the size and shape of the footplate from a micrograph by Guinan and Peake (1967). They determined the location and orientation of the footplate from a computer reconstruction of the cat middle ear (Funnell *et al.*, 1989; Funnell *et al.*, 1992). The footplate model is 20  $\mu\text{m}$  thick in the middle and 200  $\mu\text{m}$  thick at the rim and has an area of 1.16  $\text{mm}^2$ . It has a Young's modulus of  $2 \times 10^{10}$  Pa and a Poisson's ratio of 0.3.

### 5.2.2 Loading and Geometry

The stapedial footplate fits in the oval window of the cochlea. The annular ligament seals the footplate to the oval window. At low frequencies, the cochlear load acting upon the footplate is stiffness-dominated (Lynch *et al.*, 1982); this stiffness is largely the result of the annular ligament. In this model, the annular ligament is modelled by out-of-plane and in-plane springs attached along the circumference of the footplate (Ladak and Funnell, 1993); the shearing motion due to in-plane rotation of the footplate is disregarded.

The springs which limit the out-of-plane motion of the footplate are perpendicular to the plane of the footplate; one spring is attached to each of the evenly spaced nodes around the periphery of the footplate (Ladak and Funnell 1994; Ladak and Funnell, 1996). Ladak and Funnell (1994) determined the stiffness of each spring from the data of Lynch

*et al.* (1982); they found the acoustic compliance of the stapediocochlear complex to be  $0.36 \times 10^{-9} \text{ cm}^5/\text{dyn}$ . This translates to a mechanical stiffness of  $4.4 \times 10^5 \text{ dyn/cm}$ , equally distributed among the uniformly-spaced springs around the border of the footplate.

The in-plane springs are perpendicular to the rim of the footplate but are in its plane ( $x$ - $y$  plane) (Ladak and Funnell, 1996). Their purpose is to limit the in-plane motion of the footplate; they represent the in-plane stiffness of the annular ligament. Similar to the out-of-plane springs, each in-plane spring is connected to an external node on the circumference of the footplate.

The dimensions of the annular ligament are taken to be uniform around its circumference (Guinan and Peake, 1967). Ladak and Funnell (1996) calculated the stiffness of the segments (the portion between two nodes) and divided it equally between the springs at the two nodes. They considered a section of the annular ligament between two adjacent external nodes to be a "slab of uniform rectangular cross-sectional area"; its stiffness  $k_i$  can then be calculated by the following equation:

$$k_i = Etl/w,$$

where  $E$  is the Young's modulus and is  $10^5 \text{ dyn/cm}^2$  or  $10^4 \text{ Pa}$  (Lynch *et al.*, 1982),  $t$  is the thickness (equal to  $200\mu\text{m}$ ),  $l_i$  is the distance between adjacent nodes, and  $w$  is the width (equal to  $20 \mu\text{m}$ ).

There is no explicit representation of the ligaments which support the ossicular chain. However, the loading of the ossicular chain due to the ligaments is modelled by a lumped rotational stiffness of  $10^4 \text{ dyn cm}$  at a fixed axis of rotation. Ladak and Funnell (1996) obtained this sum by taking the total angular stiffness about the axis in the model of Funnell and Laszlo (1978), which was  $28 \times 10^3 \text{ dyn cm}$  and deducting the value for the angular stiffness of the cochlea ( $18 \times 10^3 \text{ dyn cm}$ ). The contributions of the anterior

malleal process and the posterior incudal ligament are represented by this stiffness. A fixed axis of rotation is assumed since it is valid at low frequencies (Guinan and Peake, 1967; Decraemer *et al.*, 1991). The axis of rotation is taken to lie in the plane of the tympanic ring and, with the exception of the rotation around the axis, all degrees of freedom on the axis are constrained to be zero.

The tensor tympani and the stapedius muscle are not represented in this middle-ear model. This is similar to simulating the condition found when the middle-ear muscles are relaxed in temporal-bone preparations and in anesthetized animals (Ladak and Funnell, 1996). The model does not include an acoustical load which would be due to the middle-ear air cavities; this is comparable to an experimental condition in which the middle-ear cavities and septum are completely opened.

### 5.3 ACOUSTIC STIMULUS

Acoustic stimulus in real life is input through the ear canal to the eardrum. It has been shown that at high frequencies the pressure distribution over the surface of the eardrum is not uniform (Stinson, 1985); however, the exact distribution is not known (Funnell *et al.*, 1987). At low frequencies, this pressure is uniform. In this model, this has been represented by an evenly distributed pressure of 100 dB SPL (or 2.828 Pa) applied to the lateral surface of the eardrum. In order to represent this in the finite-element model, the pressure is simulated by a set of forces which are normal to the surface of the eardrum.

### 5.4 BANDWIDTH MINIMIZATION

The representation of the incudostapedial joint was added to an already existing finite-element model of the middle ear (Ladak, 1993), which included structures which were represented by triangular meshes: the eardrum, manubrium, malleus, incus, crura, and footplate. Mesh generation often results in large bandwidths; therefore, after adding the new nodes and elements, a bandwidth minimization program was executed (Funnell,

1983). This program reduces the bandwidth of the system stiffness matrix by renumbering the nodes.

## 5.5 RANGE OF VALIDITY AND MODEL LIMITATIONS

The assumption of linearity limits the range of validity of this model. In addition, damping and inertial effects were omitted in this model, which limits the upper frequency for which the model is valid. Guinan and Peake (1967) found that the cochlear load causes the behaviour of the intact cat middle ear to vary only above 300 Hz. They also found that the middle ear remains linear for sound pressure levels below 130 dB SPL; this indicates that the assumption of linearity in this model is valid for normal pressure levels and for low frequencies.

Finally, one last possible limiting factor to the displacements in the model is that the displacements of the structures modelled with thin-shell or thin-plate elements must be small compared to the thickness of the structure. Unless this holds true, it is not possible to assume that the in-plane and out-of-plane displacements are not coupled. In this model, the largest footplate and eardrum displacements are about 0.5 % and 0.75% of the thickness of each respective structure; thus we can conclude that the thin-plate assumption is justified.

## CHAPTER 6. RESULTS

### 6.1 DISPLACEMENTS OF THE FOOTPLATE

#### 6.1.1 Introduction

As mentioned in Chapter 5, the model is oriented such that the footplate lies in the  $x$ - $y$  plane, with the  $x$ -axis running antero-posteriorly. The displacements at four nodes of the footplate were studied; the anterior and posterior nodes lie on the  $x$ -axis and the superior and inferior nodes lie on the  $y$ -axis. The  $x$ ,  $y$ , and  $z$  displacements of these four nodes are used to define footplate motion. Figure 6.1 on the next page shows the footplate and these four nodes.

#### 6.1.2 $X$ Displacements

As stated above, the footplate is in the  $x$ - $y$  plane; thus both the  $x$  and  $y$  displacements of the anterior, posterior, inferior and superior nodes are in-plane displacements while the  $z$  displacement is the out-of-plane displacement.

Figure 6.2 shows the  $x$  displacements of the footplate. All of the displacements increase as the incudostapedial joint becomes stiffer (as the Young's modulus of the elements representing the joint increases). The  $x$  displacements are approximately constant for Young's modulus values above  $10^{12}$  Pa and they approach zero as the joint becomes extremely flexible. This is what is expected; when the joint is very flexible (as the Young's modulus approaches zero), the stapediocochlear load is effectively decoupled from the incus. The middle-ear structures lateral to the incudostapedial joint are then "allowed" to displace more, and the stapes displacement approaches zero. In the limit, when the joint is very rigid, the  $x$  displacements are the same as those obtained for a finite-element model in which the incudostapedial joint is perfectly rigid (Ladak and Funnell, 1996).

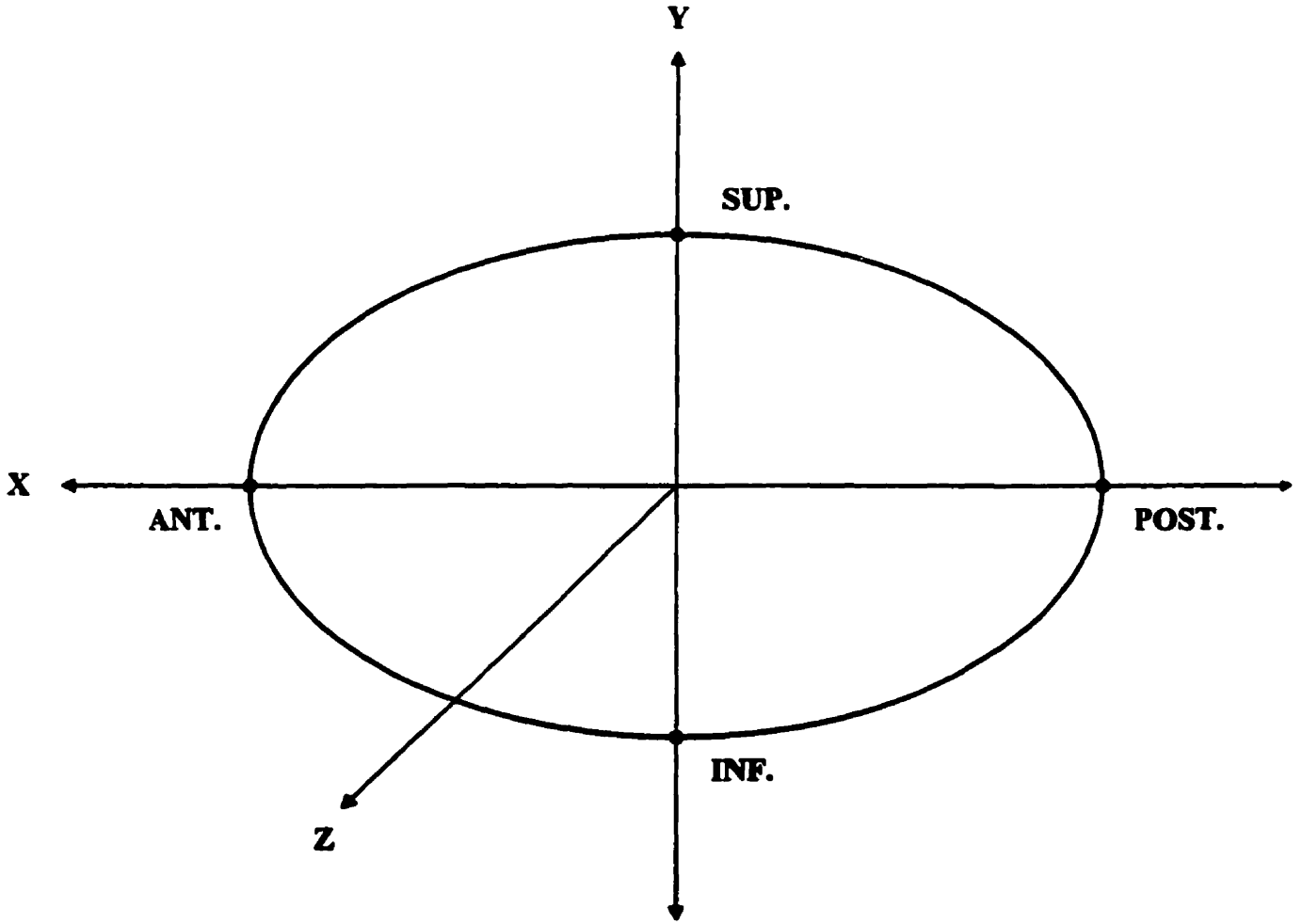


**Figure 6.1** Footplate in *x-y* plane with anterior, posterior, superior and inferior nodes.

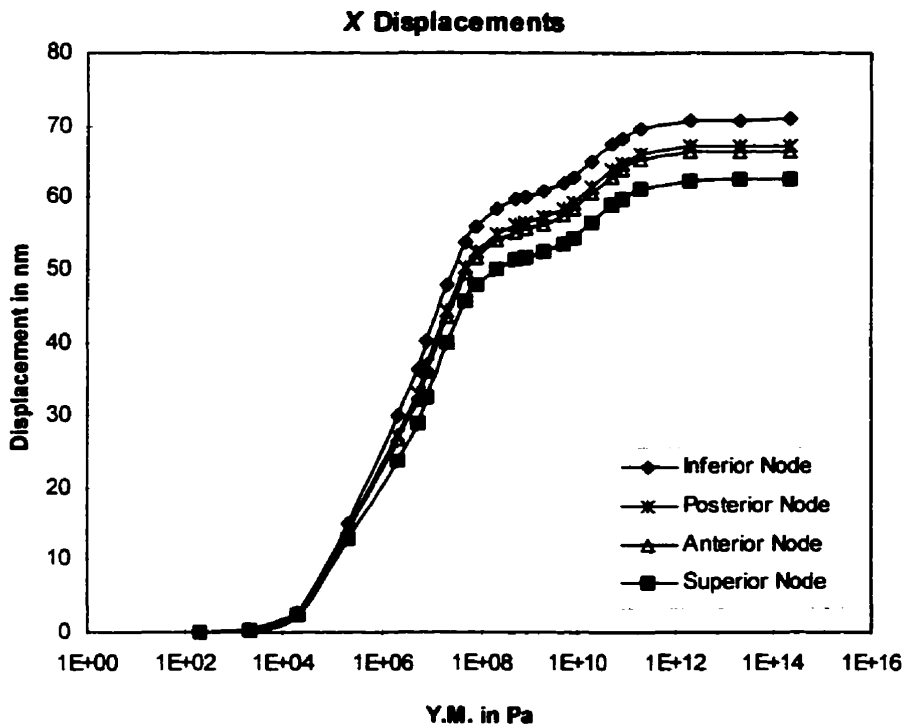


**Figure 6.2** X displacements of the footplate.

### 6.1.3 Y Displacements

The  $y$  displacements (shown in Figure 6.3) reach a plateau when the Young's modulus is greater than about  $10^9$  Pa and decrease monotonically as the joint becomes more flexible; the displacements approach zero as the Young's modulus approaches zero. Again, this is what is expected (see discussion above). As for the  $x$  displacements, in the limit, when the joint is very rigid, the  $y$  displacements are the same as those obtained for a finite-element model in which the incudostapedial joint is perfectly rigid (Ladak and Funnell, 1996).

The in-plane rotation of the footplate is given by the difference between the  $y$  displacements of the anterior and posterior nodes. It is greatest when the incudostapedial joint is effectively rigid.

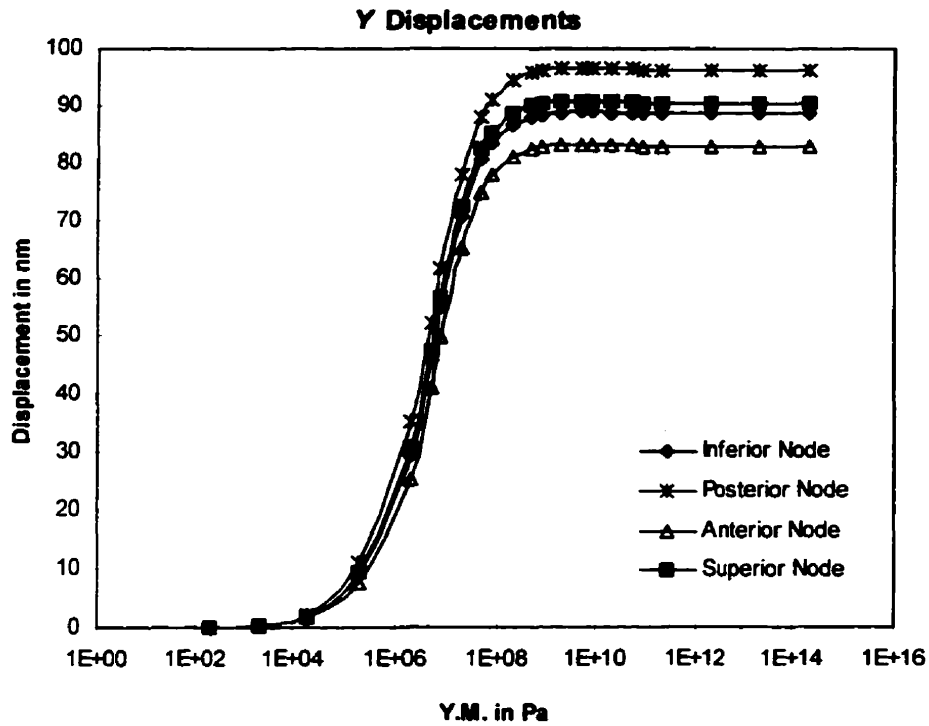


**Figure 6.3** Y displacements of the footplate.

#### 6.1.4 Z Displacements

As previously stated, the footplate lies in the  $x$ - $y$  plane and therefore the  $z$  displacement of the footplate is the out-of-plane displacement. The  $z$  displacement is the most important component of footplate displacement because it is the effective input to the cochlea. The  $z$  displacements of the anterior, posterior, inferior and superior nodes are shown in Figure 6.4.

The  $z$  displacements are approximately constant for Young's modulus values greater than about  $10^{11}$  Pa and approach zero as the Young's modulus approaches zero. Again, this is what is expected (see discussion above). Once again, in the limit, when the Young's modulus is high and the joint is effectively rigid, the  $z$  displacements are the same as

those obtained for a finite-element model in which the incudostapedial joint is perfectly rigid (Ladak and Funnell, 1996).

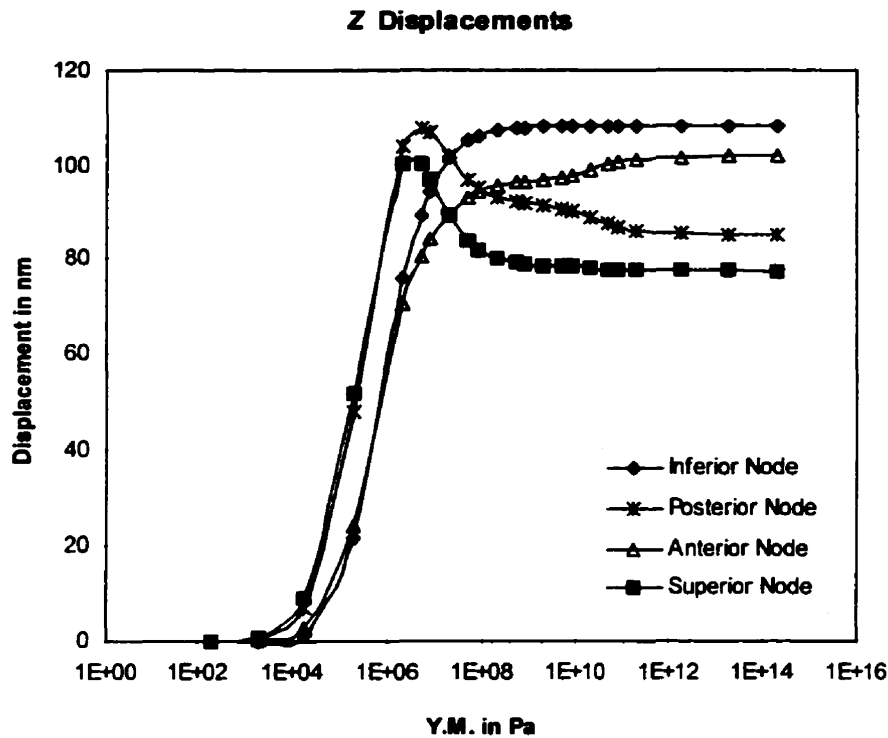


**Figure 6.4** Z displacements of the footplate.

The difference between the z displacements of the anterior and posterior nodes is proportional to the tilting of the footplate about the y-axis (antero-posterior tilting). The antero-posterior tilting of the footplate increases as the Young's modulus increases from  $2 \times 10^2$  up to about  $2 \times 10^6$  Pa; from  $2 \times 10^6$  to about  $9.5 \times 10^7$  Pa, the antero-posterior tilting decreases. At  $9.5 \times 10^7$  Pa, the anterior and posterior z displacements are equal, which means that there is no antero-posterior tilting of the footplate. After this point, the footplate starts to tilt again, but in the opposite direction. The tilting increases from this point, as the joint becomes more rigid. The greatest amount of antero-posterior tilting

occurs at a Young's modulus of about  $2 \times 10^6$  Pa; when the joint is most rigid, the tilting of the footplate is only about half as great, but in the opposite direction.

Infero-superior tilting of the footplate (tilting of the footplate about the  $x$ -axis) is proportional to the difference between the  $z$  displacements of the inferior and superior nodes. At a Young's modulus of about  $8.5 \times 10^6$  Pa, there is no infero-superior tilting of the footplate; the inferior and superior displacements are equal. The infero-superior tilting of the footplate increases as the Young's modulus increases from  $2 \times 10^2$  to about  $2 \times 10^5$  Pa; from  $2 \times 10^5$  to about  $8.5 \times 10^6$  Pa, the infero-superior tilting decreases. Then the infero-superior tilting resumes in a different direction; from approximately  $8.5 \times 10^6$  to  $8 \times 10^8$  Pa, the tilting again increases. The magnitude of the infero-superior tilt is greatest at about  $2 \times 10^5$  Pa and again when the joint is very rigid; the magnitude of the tilt is approximately equal at these points, but the tilting occurs in opposite directions.

## 6.2 DISPLACEMENTS OF THE INCUDOSTAPEDIAL JOINT

### 6.2.1 Introduction

The displacements of the nodes on the incus side of the incudostapedial joint and on the stapes side of the joint were studied. As discussed in Chapter 4, the incudostapedial joint has eight nodes, four on the stapes side and four on the incus side; the  $x$ ,  $y$ , and  $z$  displacements of these eight nodes are used to examine the motion of the joint. The four nodes on each side of the joint are: PSN, posterosuperior node; PIN, posteroinferior node; ASN, anterosuperior node; and AIN, anteroinferior node.

### 6.2.2 $X$ and $Y$ Displacements of Incus-Side Nodes

The  $x$  and  $y$  displacements of the nodes on the incus side of the incudostapedial joint are constant when the joint is extremely flexible, then decrease monotonically. When the

Young's modulus is greater than about  $10^8$  Pa, the displacements become constant. Figures 6.5 and 6.6 show the x and y displacements of the incus-side nodes, respectively.

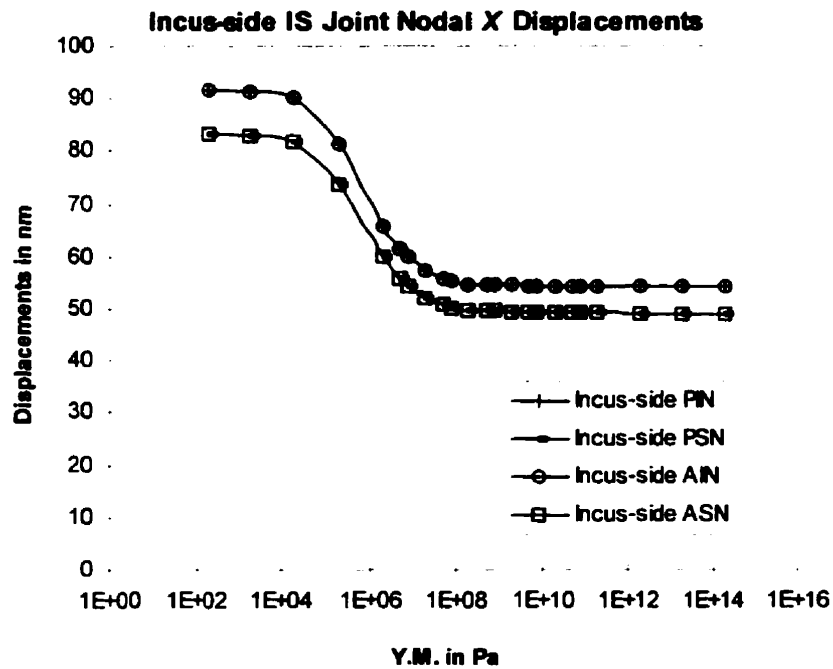
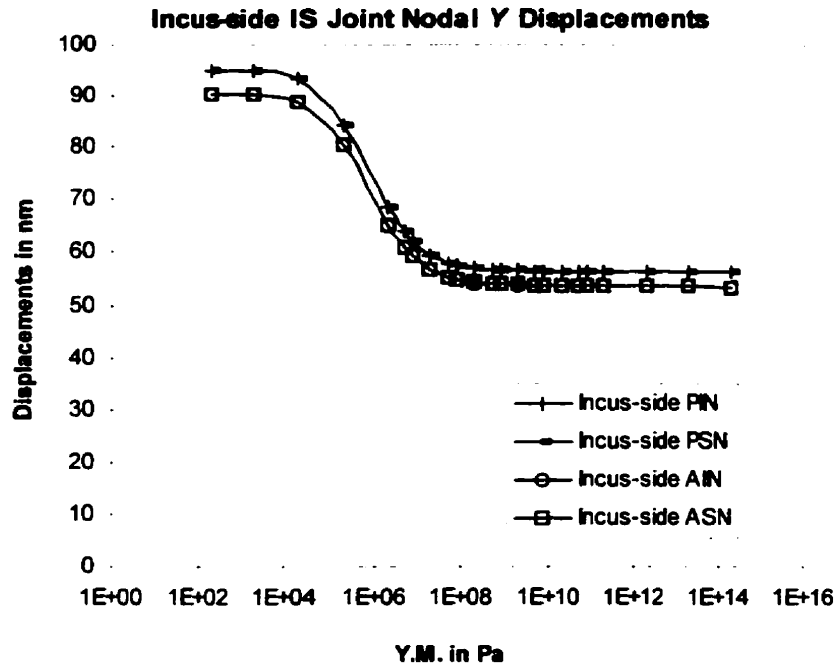


Figure 6.5 Incus-side incudostapedial joint nodal x displacements.



**Figure 6.6** Incus-side incudostapedial joint nodal y displacements.

### 6.2.3 Z Displacements of Incus-Side Nodes

The  $z$  displacements of the incus-side nodes of the incudostapedial joint are constant when the joint is extremely flexible, and again reach a plateau when the Young's modulus is greater than about  $10^8$  Pa. The displacements decrease monotonically below  $10^8$  Pa. When the Young's modulus is very high, the  $z$  displacements on both sides of the joint should track the footplate motion exactly (allowing for overall geometry). This results from the fact that at a very high Young's modulus, both the joint and the footplate move as rigid bodies joined by cortical bone (the head and crura of the stapes); thus their displacements should be almost identical. The  $z$  displacements on this side of the joint are very close to that of the footplate and are shown in Figure 6.7.

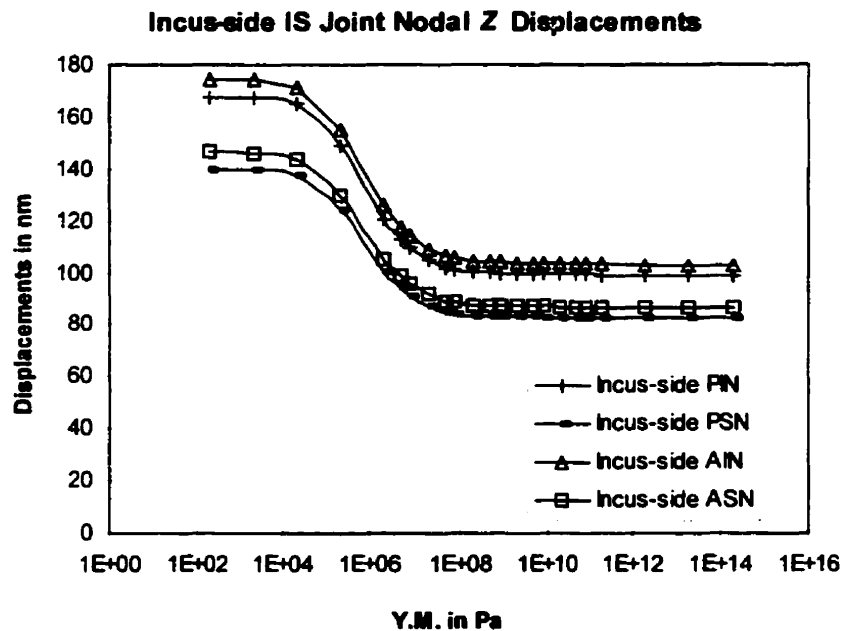


**Figure 6.7** Incus-side incudostapedial joint nodal  $z$  displacements.

#### 6.2.4 X and Y Displacements of Stapes-Side Nodes

The  $x$  displacements of the stapes-side nodes of the joint increase rapidly as the Young's modulus increases to approximately  $5 \times 10^6$  Pa; this is opposite to the way in which the joint displaces on the incus side of the joint in the  $x$  direction. After this point, they decrease slightly and finally plateau at a Young's modulus of about  $10^8$  Pa, which is again opposite to the way the joint displaces on the incus side. Figure 6.8 shows the  $x$  displacements of the stapes-side nodes.

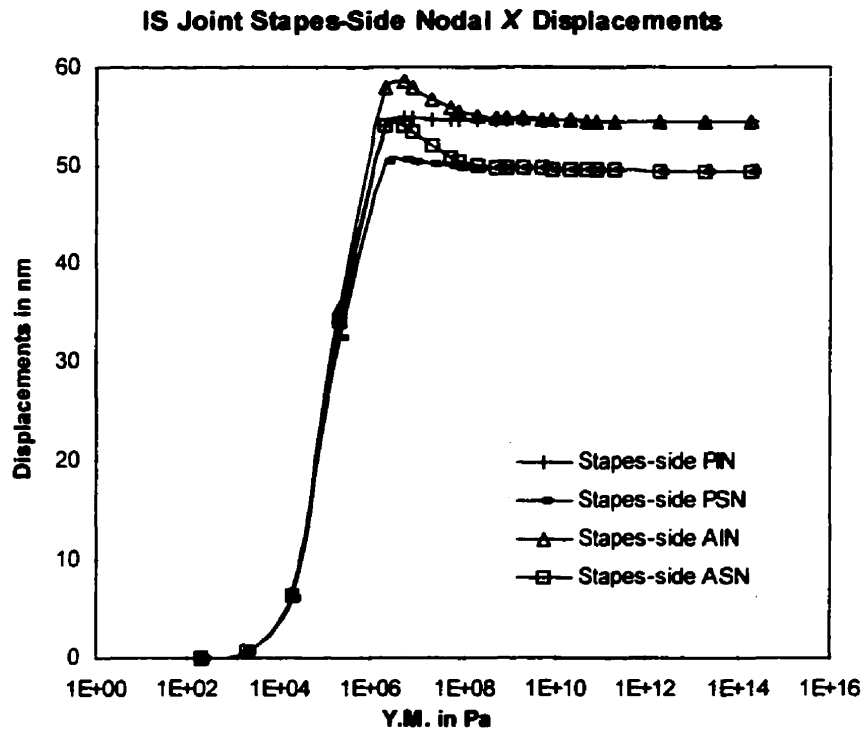
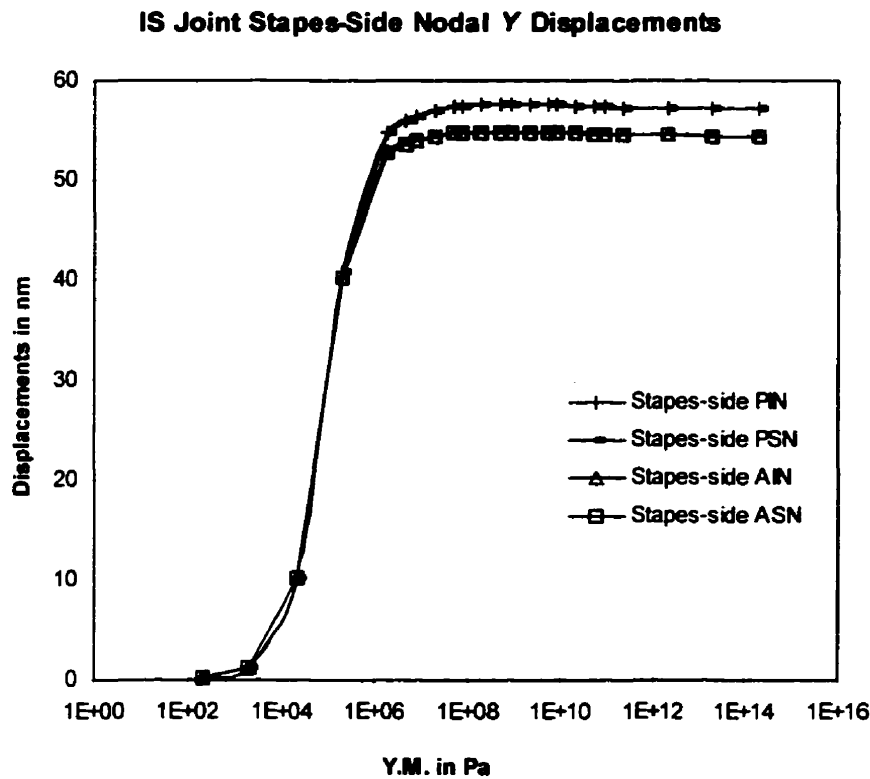


Figure 6.8 Stapes-side incudostapedial joint nodal  $x$  displacements.

The  $y$  displacements of the nodes on the incus side of the incudostapedial joint are constant when the joint is extremely flexible, then decrease monotonically. Once again, these are opposite to the displacement trends on the incus side of the joint. When the

Young's modulus is greater than about  $10^8$ , the displacements become constant, as shown in Figure 6.9. Thus, for both the  $x$  and  $y$  displacements, the stapes-side motion of the joint increases when the incus-side motion decreases and vice versa; both sides have a constant displacement when the joint is very flexible and also when the Young's modulus is greater than approximately  $10^8$  Pa.



**Figure 6.9** Stapes-side incudostapedial joint nodal  $y$  displacements.

### 6.2.5 Z Displacements of Stapes-Side Nodes

The  $z$  displacements of the nodes on the stapes side of the incudostapedial joint look somewhat similar to those of the footplate. They are constant when the joint is extremely flexible, and again reach a plateau when the Young's modulus is greater than about  $10^{12}$

Pa. As discussed previously, the  $z$  displacements on both sides of the joint should track the footplate motion exactly (allowing for overall geometry) when the Young's modulus is very high. Their displacements are almost identical for a large range of stiffness values. The  $z$  displacements on this side of the joint are shown in Figure 6.10.

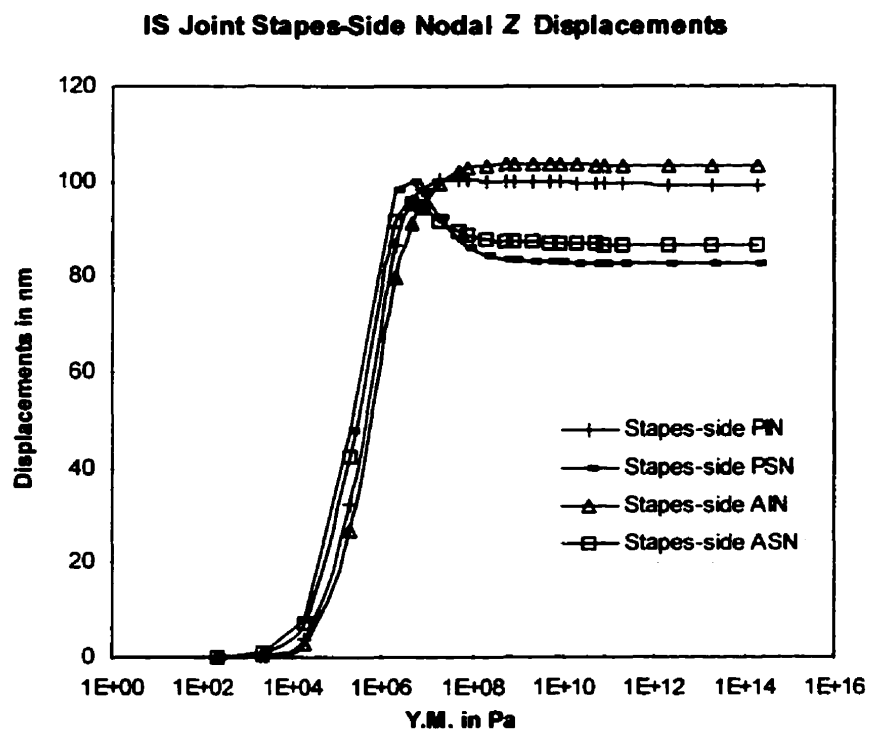


**Figure 6.10** Stapes-side incudostapedial joint nodal  $z$  displacements.

The difference between the  $z$  displacements of the joint on the incus and stapes sides is a measure of the amount of compression of the joint. The joint compresses most when it is extremely flexible. The joint compression decreases as the joint becomes less flexible. The joint does not compress at all at Young's modulus values greater than approximately  $2 \times 10^{10}$  Pa. Figure 6.11 shows the nodal compressions of the incudostapedial joint.

### Compression of the IS Joint

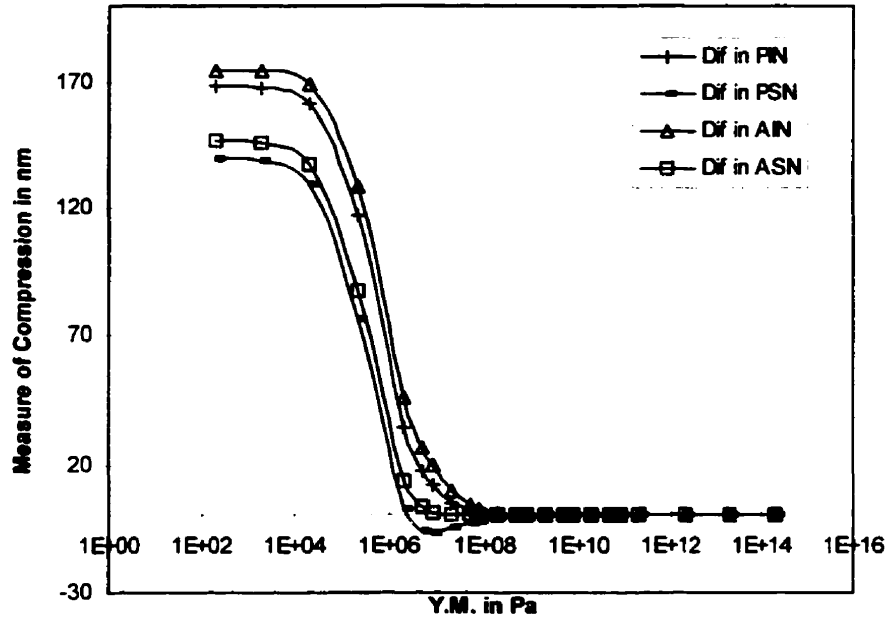
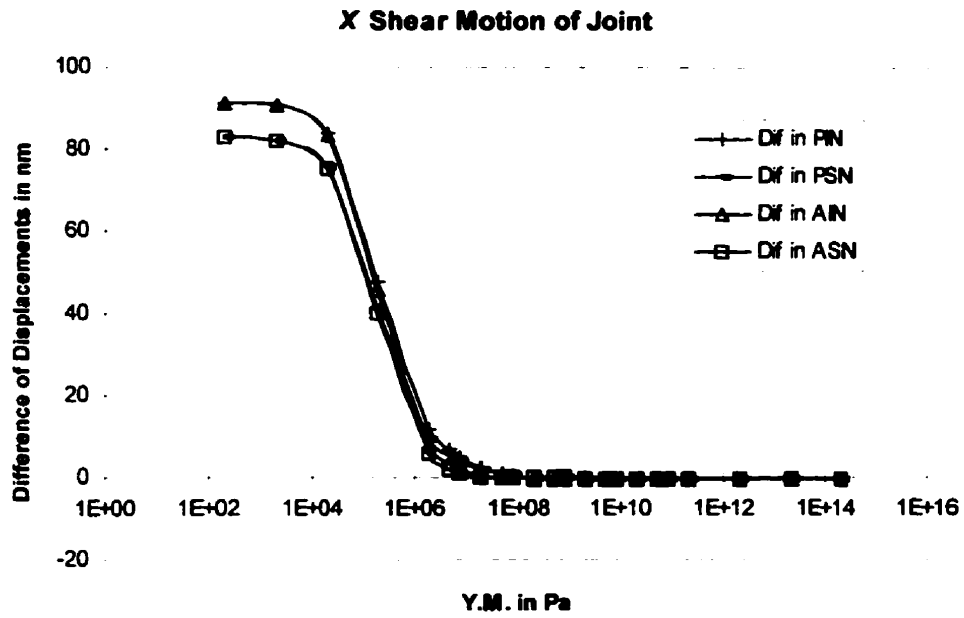


Figure 6.11 Incudostapedial joint nodal compression.

#### 6.2.6 Joint Compression vs. Joint Shear

The joint compression is greater than the joint shear. The difference between the  $x$  displacements of the joint is a measure of the  $x$  shear and the difference between the  $y$  displacements of the joint is a measure of the  $y$  shear. Figures 6.12 and 6.13 show the  $x$  and  $y$  shear, respectively. The  $x$  and  $y$  shear are comparable for all Young's modulus values.



**Figure 6.12** X Shear of the incudostapedial joint.

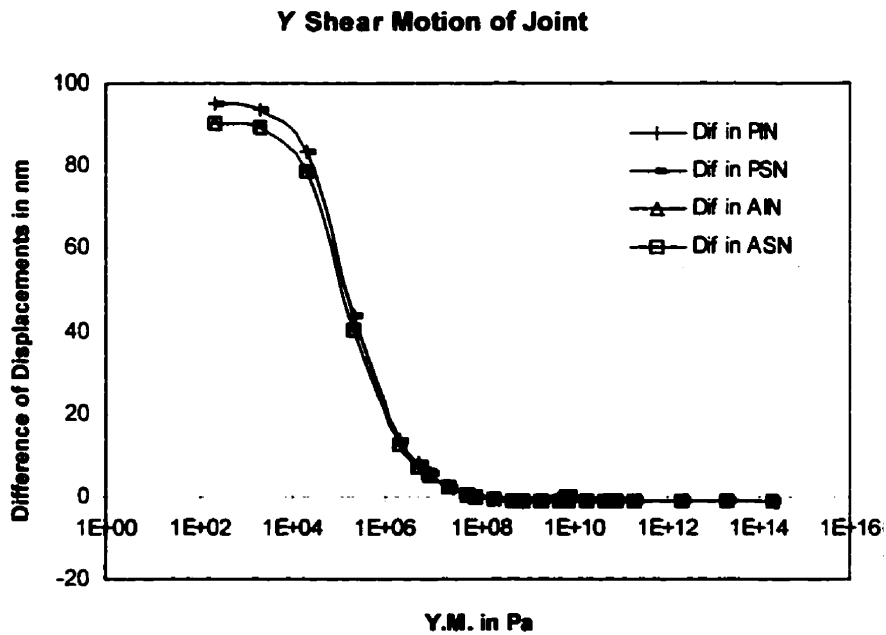


**Figure 6.13** Y Shear of the incudostapedial joint.

### 6.2.7 Range of Validity

One potential limit to the range of displacements for which the model is valid is due to a constraint that all thin-shell and thin-plate elements have, namely that the displacements must be small compared to the thickness of the structure itself. Thus, the joint must displace much less than the dimensions of the joint itself. The dimensions of the joint are  $300 \times 10^3$  nm by  $552 \times 10^3$  nm by  $35 \times 10^3$  (x by y by z). The maximum relative displacement of the joint nodes in the x direction is about 90 nm, which is 0.0001% of the total x dimension of the joint. In the y direction, the maximum relative displacement of the joint nodes is 95 nm, which is 0.017% of the total y dimension of the joint. The maximum relative displacement of the joint nodes in the z direction is 175 nm, which is 0.5% of the total z dimension of the joint. Thus, since the joint displaces much less in each direction compared to the dimension in that direction, the range of displacements seem reasonable and valid.

### 6.2.8 Assumption of Linearity

The assumption of linearity in this model can be validated if the maximum compression of the joint is much less than the dimensions of the joint. The maximum compression of the joint is 175 nm, which is 0.5% of the z dimension of the joint. Thus the compression of the joint is small compared to the z dimension of the joint, and the assumption of linearity holds for the model.

## 6.3 EARDRUM AND MANUBRIAL DISPLACEMENTS

### 6.3.1 Introduction

The maximum drum displacements and maximum manubrial displacements were studied. As discussed in Chapter 2, the manubrium is the part of the malleus which is attached to

the eardrum. The manubrium is actually dense cortical bone while the eardrum is a membrane.

### 6.3.2 Maximum Drum and Manubrial Displacements

The maximum drum displacements and maximum manubrial displacements (shown in Figure 6.14) can be used to characterize drum and manubrium movements. Both drum and manubrial displacements decrease monotonically as the Young's modulus of the shell

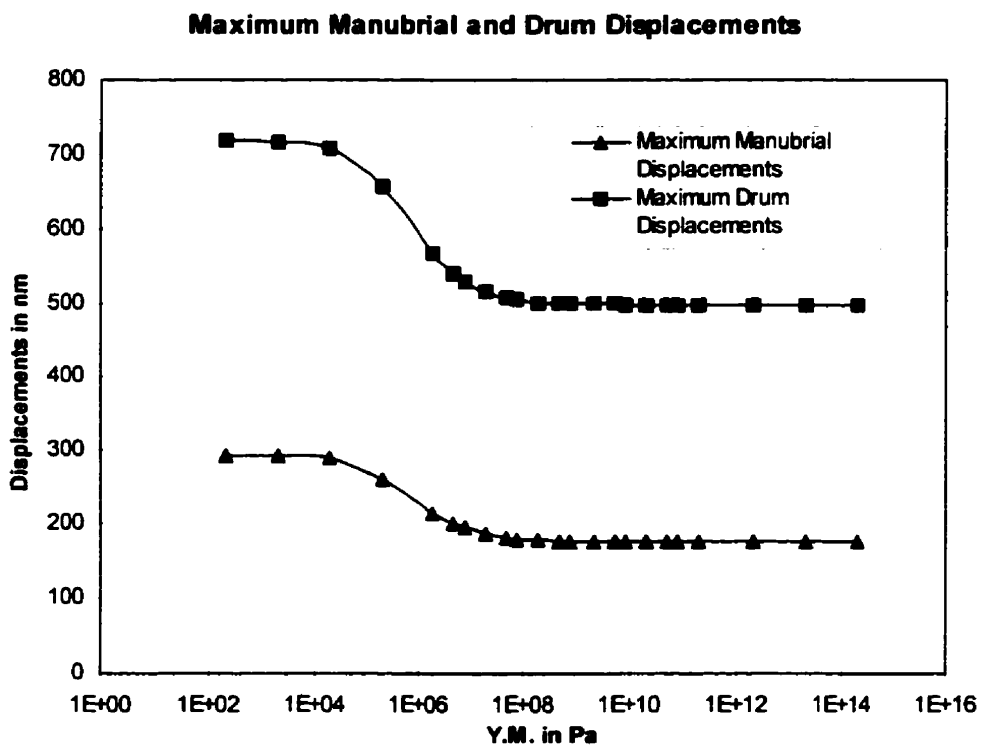


**Figure 6.14** Eardrum and manubrial displacements.

elements representing the joint increases. They are constant at high Young's modulus values and low Young's modulus values. For any given joint stiffness, the drum displaces over twice as much as the manubrium. The periphery of the drum is clamped and does not move at all. When the Young's modulus is very low, the maximum drum

manubrial displacements are 67% and 45% greater, respectively, than when the Young's modulus is very high.

### 6.3.3 Vibration Patterns on the Eardrum

A change in the ratio of maximal umbo (the deepest point in the drum, corresponding to the manubrium) displacement to maximal drum displacement implies that the vibration pattern on the eardrum has changed. When the joint is very flexible, the ratio between the maximum drum displacements and maximum manubrial displacements is about 2.5; when the joint is most rigid, this ratio increases to 2.8, which implies that the vibration pattern has changed slightly. The vibration patterns for Young's moduli of  $2 \times 10^3$ ,  $2 \times 10^6$  and  $2 \times 10^{13}$  follow.

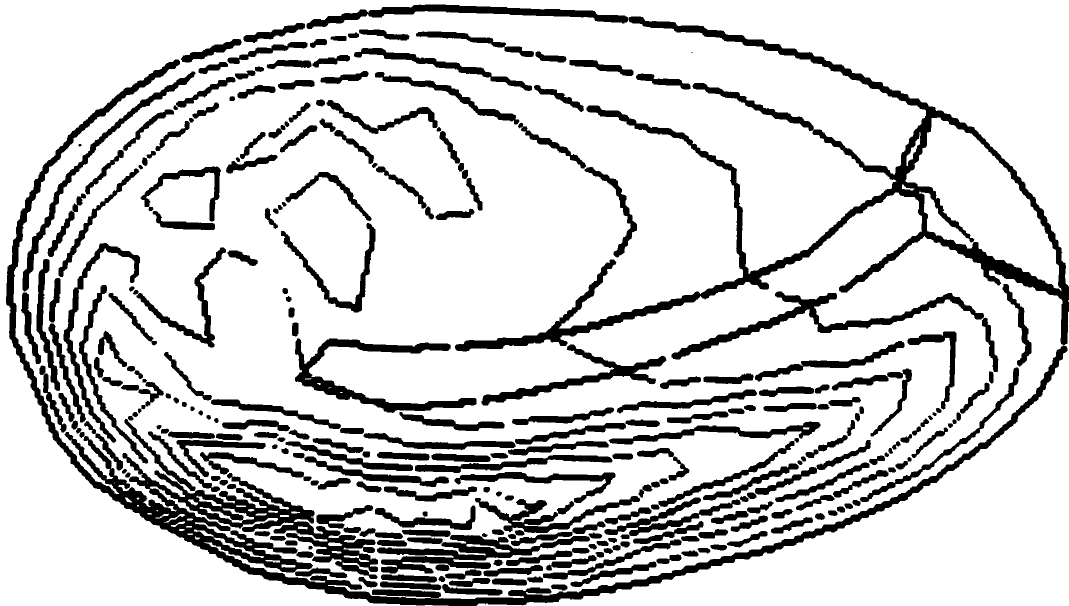


**Figure 6.15** Eardrum vibration patterns for a Young's modulus of  $2 \times 10^3$ ; maximum drum displacement: 717.8 nm.

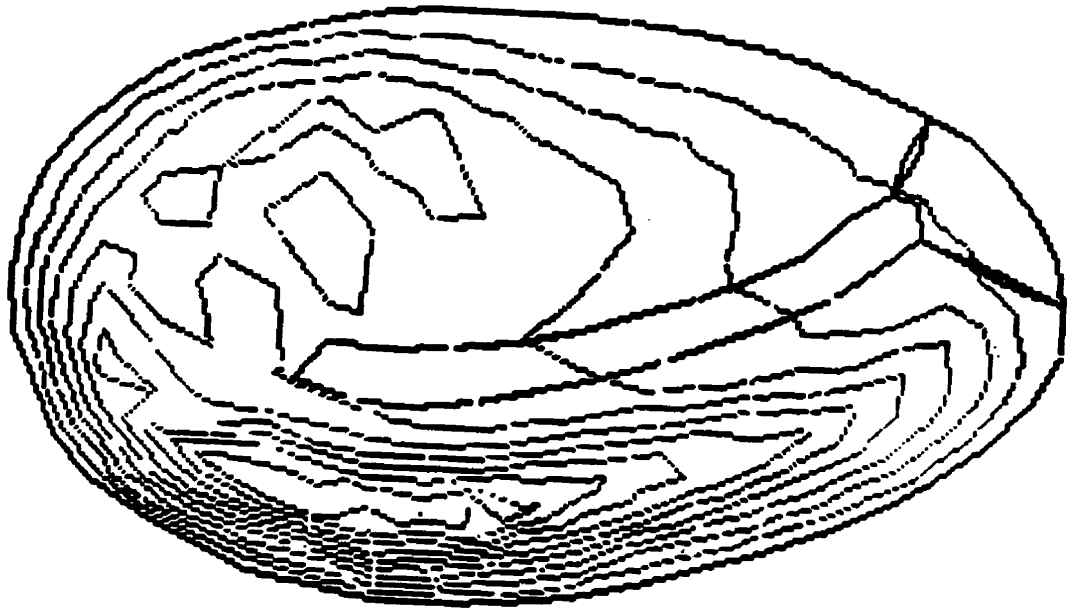


**Figure 6.16** Eardrum vibration patterns for a Young's modulus of  $2 \times 10^6$ ; maximum drum displacement: 657.3 nm.

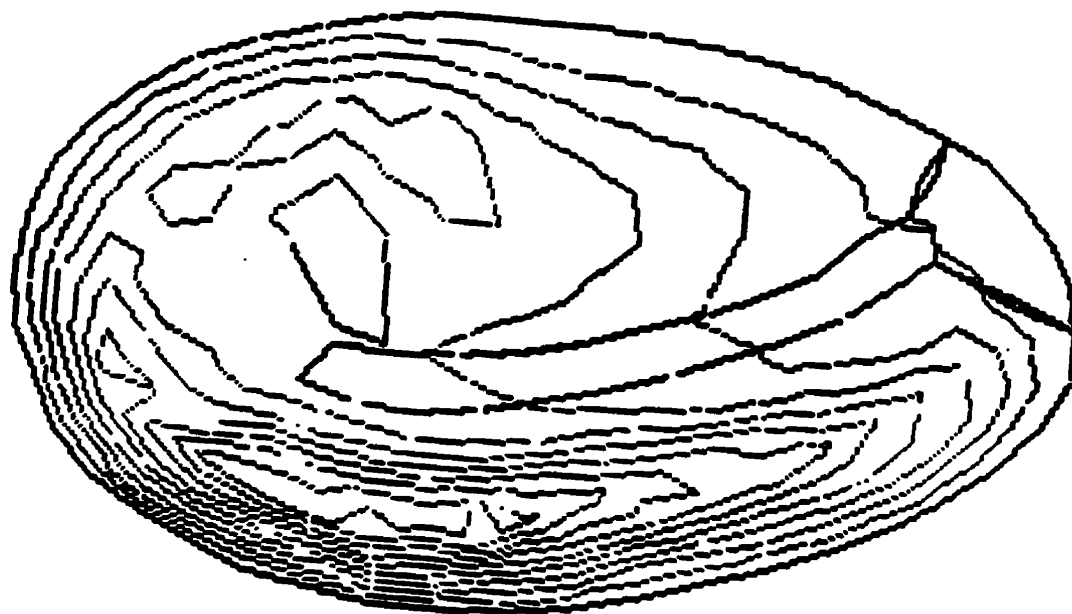


**Figure 6.17** Eardrum vibration patterns for a Young's modulus of  $2 \times 10^{13}$ ; maximum drum displacement: 496.7 nm.

## 6.4 CONCLUSION

The displacements of the footplate, incudostapedial joint, eardrum and manubrium behave as expected in this model. When the static pressure is applied to the eardrum, the manubrium pushes on the rigid incudomalleolar structure, which in turn pushes on one side of the elastic incudostapedial joint. The other side of the joint pushes on the head of the rigid stapes, which then pushes on the footplate. The footplate pushes on the annular ligament which is fixed to the unmoving temporal bone. If the incudostapedial joint is much stiffer than the annular ligament, the joint will not compress, and the displacement of the footplate (a rotation around the fixed axis of rotation) is the same as that of the manubrium.

When the incudostapedial joint is much more flexible than the annular ligament, the joint will compress and the annular ligament will not have to “give” much; thus the displacement of the footplate will be much less than that of the manubrium. These are the results obtained in this model. However, it is important to note that the displacements do not have to be the same at different points; the displacement of the manubrium is approximately equal to the “give” in the incudostapedial joint plus the “give” in the annular ligament.

In this model, the incudostapedial joint has only one shell across the joint-capsule thickness and along each side; therefore it behaves more stiffly than it should for a given Young’s modulus. Thus, the Young’s modulus values presented here should not be taken at face value, and a convergence test should be done using finer and finer meshes.

## **CHAPTER 7. CONCLUSIONS AND FURTHER DEVELOPMENTS**

### **7.1 CONCLUSIONS**

A finite-element model of the cat middle ear was modified to include a shell representation of the incudostapedial joint. The model was subjected to a low-frequency, uniform sound pressure applied to the lateral side of the eardrum. Joint stiffness was varied and the resulting displacements of the footplate, incudostapedial joint, manubrium and eardrum were examined.

There is a significant antero-posterior and infero-superior tilting of the footplate for almost all joint stiffnesses. The in-plane rotation of the footplate is greatest when the incudostapedial joint is effectively rigid. The joint compresses most when it is extremely flexible and the compression decreases as the joint becomes less flexible; it does not compress at all when the joint is infinitely stiff. In addition, the joint does have both  $x$  and  $y$  shear, which are less than the joint compression. These findings are consistent with the experimental results found by Guinan and Peake (1967); they found that the joint slipped sideways and compressed. They also found that the stapes had an appreciable rocking movement as well as movement in and out of the oval window, like a piston. The rocking movement that they described corresponds to the antero-posterior and infero-superior tilt found here.

The eardrum vibration pattern found here is similar to previous models. For any given joint stiffness, the eardrum displaces more than twice as much as the manubrium; in addition, the vibration pattern of the drum changes as the joint stiffness changes, but not very much.

The incudostapedial joint nodal displacements are much less than the dimensions of the joint. The ratio of the largest nodal displacement in the joint to the smallest dimension of the joint is 0.5%, which is the maximum amount of bending that occurs. This ratio

indicates that the thin-shell assumption is reasonable. When the joint is extremely rigid, the footplate displacements agree with those obtained from a previous model, where the incudostapedial joint had no explicit representation and was functionally rigid (Ladak and Funnell, 1996). When the joint is extremely flexible (as the Young's modulus approaches zero), the footplate displacements approach zero. This is what is expected: when the incudostapedial joint is much more flexible than the annular ligament, the joint will compress and the annular ligament will not have to "give" much, so the footplate displacement will be much smaller.

## 7.2 FURTHER DEVELOPMENTS AND CLINICAL APPLICATIONS

As stated in the last chapter, the incudostapedial joint in this model has only one shell element across the joint-capsule thickness and along each side, which makes the joint behave more stiffly than it should for a given Young's modulus. The Young's modulus values presented here provide a measure of the joint stiffness, but are not a property of the joint. A convergence test should be done using finer and finer meshes. A wide range of Young's modulus values were used in the simulations. The true Young's modulus of the incudostapedial joint most likely lies in the transition regions of the displacements, since the joint is neither very rigid nor very flexible. The dimensions of the joint were measured from one set of histological slides. The joint could be measured from other slides to get more accurate dimensions.

As stated in the previous section, a flexible incudostapedial joint was added to an existing finite-element model by Ladak and Funnell (1996). Since then, the model has been refined to include explicit ligament representations (Funnell, 1996) and an ossicular axis of rotation which is not fixed; thus, the latest version of this model now contains at least crude representations of all of the major mechanical components of the middle ear. Therefore, it can potentially serve as a basis for investigating the importance of various parameters, such as Young's modulus, shape, or thickness, in designing tympanic membrane graft material or ossicular prostheses. This model can also potentially help

guide new experimental work to measure the three-dimensional motion of the middle ear and can be used for quantitative comparison with such experimental data.

## REFERENCES

Bathe, K.-J. (1982). *Finite Element Procedures in Engineering Analysis* (Prentice-Hall, New Jersey).

Bathe, K.-J., Wilson, E.L., and Peterson, F.E. (1973). "SAP IV. A structural analysis program for static and dynamic response of linear systems," Report No. EERC 73-11 (University of California, Berkeley).

Békésy, G.v. (1960). *Experiments in Hearing*, translated and edited by E.G. Wever (McGraw-Hill Book Co., New York).

Beltzer, A.I. (1990). *Variational and Finite Element Method* (Springer-Verlag, Berlin).

Bess, F.H. and Humes, L.E. (1995). *Audiology: The Fundamentals* 2nd. Ed. (Williams and Wilkins, Baltimore).

Calcaterra, T.C., Gussen, R. and Schwartz, H.E. (1972). "Ossicular joint healing: an experimental study." *Ann. Otol. Rhino. Laryng.* **81**, 690-694.

Cook, R.D., Malkus, D.S., and Plesha, M.E. (1989). *Concepts and Applications of Finite Element Analysis*, 3rd ed. (John Wiley and Sons, New York).

Dankbaar, W.A. (1970). "The pattern of stapedial vibration," *J. Acoust. Soc. Am.* **48**, 1021-1022.

Decraemer, W.F., and Khanna, S.M. (1993). "Malleus motion in guinea pig ear measured with a heterodyne interferometer," *Abstracts 16th Annual Midwinter Mtg. Assoc. Research Otol.*, **13**.

Decraemer, W.F., Dirckx, J.J.J., and Funnell, W.R.J. (1991). Shape and derived geometrical parameters of the adult, human tympanic membrane measured with a phase shift moire interferometer *Hear. Res.* **51**, 107-122.

Decraemer, W.F., Khanna, S.M., and Funnell, W.R.J. (1989). "Interferometric measurement of the amplitude and phase of tympanic membrane vibrations in cat," *Hear. Res.* **38**, 1-18.

Decraemer, W.F., Khanna, S.M., and Funnell, W.R.J. (1991). "Malleus vibration mode changes with frequency," *Hear. Res.* **54**, 305-318.

Desai, C.S. and Abel, J.F. (1972). *Introduction to the Finite-Element Method: A Numerical Method for Engineering Analysis* (Van Nostrand Reinhold, New York).

Donaldson, J.A., Duckert, L.G., Lambert, P.M., and Rubel, E.W. (1992). *Surgical Anatomy of the Temporal Bone*, 4th ed. (Raven Press, New York).

El-Mofty, A and El-Serafy, S. (1968). "The ossicular chain in mammals," *Ann. Oto. Rhino. Laryng.* **76**, 903-907.

Esser, M.H.M. (1947). "The mechanism of the middle ear: II. The drum," *Bull. Math. Biophys.* **9**, 75-91.

Fumigalli, Z. (1949). "Morphological research on the sound-transmission apparatus," *Arch. Ital. Otol. Rinol. Laringol. (Suppl. 1)* **60**, pp. 1-323 (in Italian).

Funnell, S.M. (1989). *An Approach to Finite-Element Modelling of the Middle Ear* (Master's Thesis, McGill University, Montréal).

Funnell, W. R. J. and Laszlo, C.A. (1982). "A critical review of experimental observations on ear-drum structure and function" *Otorhinolaryngology (ORL)* **44**, 181-205.

Funnell, W.R.J. (1972). *The Acoustical Impedance of the Guinea-Pig Middle Ear and the Effects of the Middle-Ear Muscles* (Master's Thesis, McGill University, Montréal).

Funnell, W.R.J. (1975). *A Theoretical Study of Eardrum Vibrations Using the Finite-Element Method* (Ph.D.Thesis, McGill University, Montréal).

Funnell, W.R.J. (1983). "On the undamped natural frequencies and mode shapes of a finite-element model of the cat eardrum," *J. Acoust. Soc. Am.* **73**, 1657-1661.

Funnell, W.R.J. (1987). "On the damped frequency response of a finite-element model of the eardrum," *J. Acoust. Soc. Am.* **81**, pp. 1851-1859.

Funnell, W.R.J. and Laszlo, Charles A., (1978). "Modeling of the cat eardrum as a thin shell using the finite-element method," *J. Acoust. Soc. Am.* **63**, 1461-1467.

Funnell, W.R.J., Khanna, S.M., and Decraemer, W.F. (1992). "On the degree of rigidity of the manubrium in a finite-element model of the cat eardrum," *J. Acoust. Soc. Am.* **91**, 2082-2090.

Funnell, W.R.J. (1983). "On the undamped natural frequencies and mode shapes of a finite-element model of the cat eardrum," *J. Acoust. Soc. Am.* **73**, 1657-1661.

Funnell, W.R.J. (1996). "Finite-element modelling of the cat middle ear with elastically suspended malleus and incus", 19th Midwinter Res. Mtg., Assoc. Res. Otolaryngol., St. Petersburg Beach.

Funnell, W.R.J. and Decraemer, W.F. (1996). "On the incorporation of moiré shape measurements in finite-element models of the cat eardrum," J. Acoust. Soc. Am., in press.

Funnell, W.R.J. (1996) "Low-frequency coupling between eardrum and manubrium in a finite-element model," J. Acoust. Soc. Am. **99**, 3036-3043.

Gallagher, R. H. (1975). *Finite element analysis: fundamentals* (Prentice-Hall, New Jersey).

Gran, S. (1968). *The analytical basis of middle-ear mechanics. A contribution to the application of the acoustical impedance of the ear.* (Dissertation, University of Oslo, Oslo) (in German).

Guinan, J. J., Jr., and Peake, W. T. (1967). "Middle ear characteristics of anesthetized cats." J. Acoust. Soc. Am, **41**, 1237-1261.

Gundersen, T. (1972). "Prostheses in the ossicular chain. I. Mechanics of movement," Arch. Otolaryng. **96**, 416-422.

Gyo, K., Aritomo, H., and Goode, R.L. (1987). "Measurement of the ossicular vibration ratio in human temporal bones by use of a video measuring system," Acta Otolaryngol. (Stockh.) **103**, 87-95.

Harneja, N.K. and Chaturvedi, R.P, (1973). "A study of the human ear ossicles," Ind. J. Otol. **25**, 154-160.

Helmholtz, H.L.F. (1869). "The mechanism of the middle-ear ossicles and of the eardrum," Pflügers Archiv. f. Physiol. (Bonn) **1**, 1-60 [in German: trans. by A.H. Buck and N. Smith (W. Wood, New York, 1873 69 pp.) and by J. Hinton, (Publ. New Sydenham Soc. London **62**, 97-155 (1874).

Høgmoen, K., and Gundersen, T. (1977). "Holographic investigation of stapes footplate movements," Acustica **37**, 198-202.

Jayne, H. (1898). *Mammalian anatomy. I. The skeleton of the cat.* (Lippincott, Philadelphia).

Katz, J. (1985). *Handbook of Clinical Audiology*, 3rd ed. (Williams and Wilkins, Baltimore).

Kessel, R.G. and Kardon, W.H. (1979). *Tissues and Organs: A Text Atlas of Scanning Electron Microscopy* (W.H. Freeman and Company).

Khanna, S.M. (1970). *A Holographic Study of Tympanic Membrane Vibrations in Cats* (Ph.D. thesis, City University of New York, New York).

Khanna, S.M., and Tonndorf, J. (1971). "The vibratory pattern of the round window," *J. Acoust. Soc. Am.* **50**, 1475-1483.

Khanna, S.M., and Tonndorf, J. (1972). "Tympanic membrane vibrations in cats studied by time-averaged holography," *J. Acoust. Soc. Am.* **51**, 1904-1920.

Kirikae, I. (1960). *The Structure and Function of the Middle Ear* (University of Tokyo Press, Tokyo).

Kobayashi, M. (1954). "On the ligaments and articulations of the tympanic ossicles of man," *Pract. Otol. (Zibi Rhinsho)* **47**, 587-593 (in Japanese).

Kobayashi, M. (1955). "The articulation of the auditory ossicles and their ligaments of various species of mammalian animals," *Hiroshima Journal of Medical Sciences* **4**, 319 - 349.

Kobrak, H.G. (1959). *The Middle Ear* (University of Chicago Press, 1959).

Ladak, H.M. (1993). *Finite-Element Modelling of Middle-Ear Prosthesis in Cat* (Master's Thesis, McGill University, Montréal).

Ladak, H.M., and Funnell, W.R.J. (1994). "Finite-element modelling of malleus-stapes and malleus-footplate prostheses in cat," 17th Midwinter Res. Mtg., Assoc. Res. Otolaryngol., St. Petersburg Beach.

Ladak, H.M., and Funnell, W.R.J. (1996). "Finite-element modeling of the normal and surgically repaired cat middle ear," *J. Acoust. Soc. Am.* **100**, 933-944.

Lesser, T.H.J., and Williams, K.R. (1988). "The tympanic membrane in cross section: a finite element analysis," *J. Laryngol. Otol.* **102**, 209-214.

Lesser, T.H.J., Williams, K.R., and Skinner, D.W. (1988). "Tympanosclerosis, grommets and shear stresses," *Clin. Otolaryngol.* **13**, 375-380.

Lesser, T.H.J., Williams, K.R., and Blayney, A.W. (1991). "Mechanics and materials in middle ear reconstruction," *Clin. Otolaryngol.* **16**, 29-32.

Lim, D.J. (1968). "Tympanic membrane. Electron microscope observation. Part I. Pars tensa," *Acta Otolaryngol.* **66**, 181-198.

Lim, D.J. (1970). "Human tympanic membrane. An ultrastructural observation," *Acta Otolaryng.* **70**, 176-186.

Lynch, T.J., III, Nedzelnitsky, V., and Peake, W.T. (1982). "Input impedance of the cochlea in cat," J. Acoust. Soc. Am. **72**, 108-130.

Møller, A.R. (1961). "Network model of the middle ear," J. Acoust. Soc. Am. **33**, 168-176.

Møller, A.R. (1963). "Transfer function of the middle ear," J. Acoust. Soc. Am. **35**, 1526-1534.

Norrie, D.H. and de Vries, G. (1973). *The Finite Element Method* (Academic Press, New York).

Norrie, D.H. and de Vries, G. (1978). *An Introduction to Finite Element Analysis* (Academic Press, NY).

Palmer, J.M. (1993). *Anatomy for Speech and Hearing*, 4th ed. (Williams and Wilkins, Baltimore).

Pickles, J.O. (1988). *An Introduction to the Physiology of Hearing* (Academic Press, San Diego).

Rabbitt, R.D. (1985). "A dynamic fiber composite continuum model of the tympanic membrane. Part I: Model Formulation," Math. Report No. 151. (Rensselaer Polytechnic Institute, Troy, New York).

Rabbitt, R.D., and Holmes, M.H. (1986). "A fibrous dynamic continuum model of the tympanic membrane," J. Acoust. Soc. Am. **80**, 1716-1728.

Relkin, E.M. (1988). "Introduction to the analysis of middle-ear function" in *Physiology of the Ear* ed. Jahn, A.F. and Santos-Sacchi, J. (Raven Press, New York), pp. 103-123.

Ross, C.T.F. (1985). *Finite Element Methods in Structural Analysis* (C.T.F. Ross/Ellis Horwood, Chichester).

Sarrat, R., Guzmán, A.G. and Torres, A. (1988). "Morphological Variations of Human Ossicula Tympani," *Acta Anatomica* **131**, 146-149.

Shaw, E.A.G., and Stinson, M.R. (1986). "Eardrum dynamics, middle ear transmission and the human hearing threshold curve," Proceedings of the 12th International Congress on Acoustics, Toronto, paper b6-6.

Schuknecht, H.F., and Gulya, A. J. (1986). *Anatomy of the Temporal Bone with Surgical Implications* (Lea & Febiger, Philadelphia).

Tonndorf, J., Khanna, S.M., and Fingerhood, B.J. (1966). "The input impedance of the inner ear in cats," *Ann. Otol. Rhino. Laryngol.* **75**, 752-763.

Tonndorf, J., and Khanna, S.M. (1970). "The role of the tympanic membrane in middle ear transmission," *Ann. Otol. Rhinol. Laryngol.* **79**, 743-753.

Tonndorf, J., and Khanna, S.M. (1971). "The tympanic membrane as a part of the middle ear transformer," *Acta Otolaryng.* **71**, 177-180.

Tonndorf, J., and Khanna, S.M. (1972). "Tympanic-membrane vibrations in human cadaver ears studied by time-averaged holography," *J. Acoust. Soc. Am.* **52**, 1221- 1233.

Tonndorf, J., and Pastaci, H. (1986). "Middle ear sound transmission: A field of early interest to Merle Lawrence," *Am. J. Otolaryngol.* **7**, 120-129.

Vlaming, M.S.M.G. (1987). *Middle Ear Mechanics Studied by Laser Doppler Interferometry* (Ph.D. thesis, Technische Universiteit Delft, Delft, The Netherlands).

Vlaming, M.S.M.G., and Feenstra, L. (1986). "Studies on the mechanics of the normal human middle ear," *Clin. Otolaryngol.* **11**, 353-363.

Wada, H., Tetsuro, M., and Kobayashi, T. (1992). "Analysis of dynamic behaviour of human middle ear using a finite-element method," *J. Acoust. Soc. Am.* **92**, 3157- 3168.

Williams, K.R., and Lesser, T.H.J. (1990). "A finite element analysis of the natural frequencies of vibration of the human tympanic membrane. Part I.," *Br. J. Audiol.* **24**, 319-327.

Wever, E.G., and Lawrence, M. (1954). *Physiological Acoustics* (Princeton University Press, New Jersey).

Wever, E.G., Lawrence, M., and Smith, K.R. (1948). "The middle ear in sound conduction," *Arch. Otolaryngol.* **49**, 19-35.

Williams, K.R., and Lesser, T.H.J. (1990). "A finite element analysis of the natural frequencies of vibration of the human tympanic membrane. Part I.," *Br. J. Audiol.* **24**, 319-327.

Williams, K.R., and Lesser, T.H.J. (1992). "A dynamic and natural frequency analysis of the Fisch II spandrel using the finite element method," *Clin. Otolaryngol.* **17**, 261- 270.

Yang, T.Y. (1986). *Finite Element Structural Analysis* (Prentice-Hall, Englewood Cliffs).

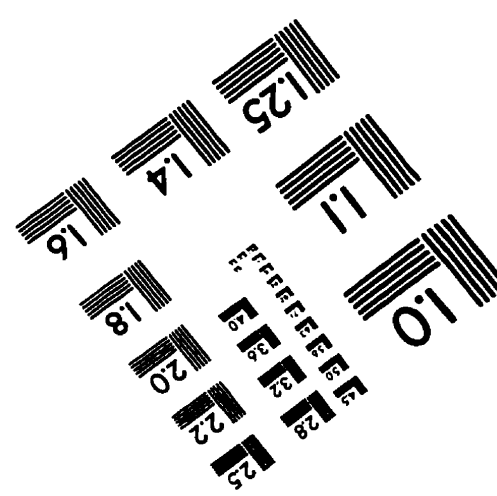
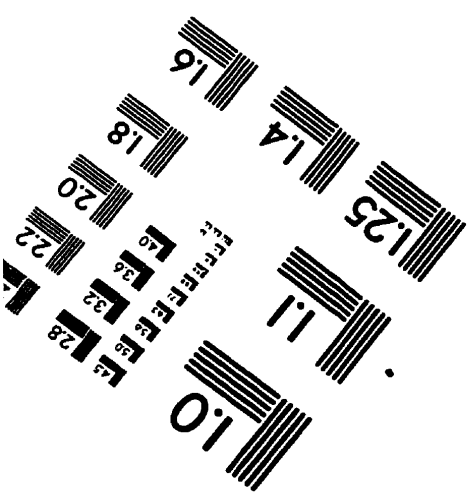
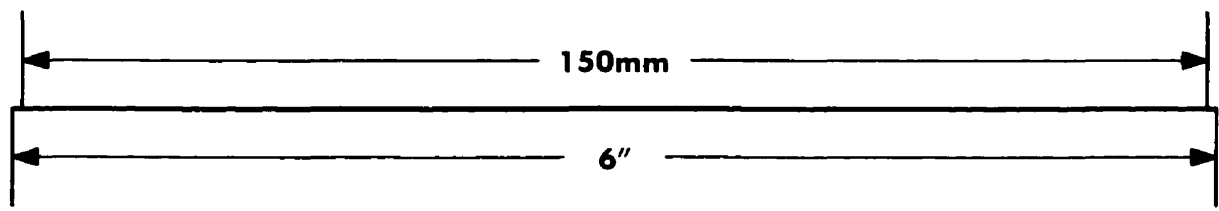
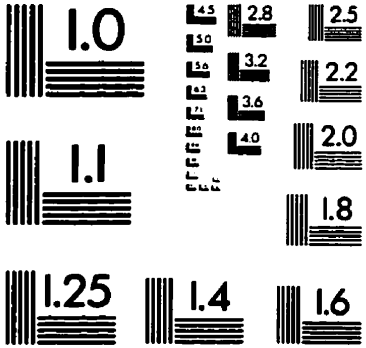
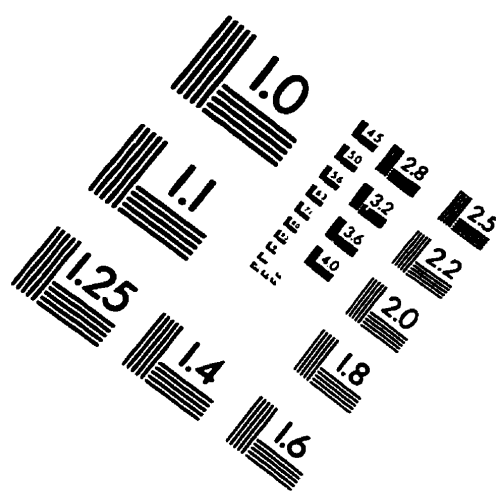
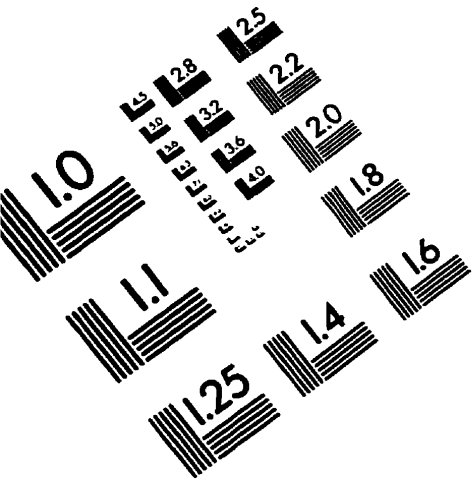
Yost, W.A. and Nielson, D.W. (1985). *Fundamentals of Hearing: An Introduction* (Holt, Rinehart and Winston, New York).

Zienkiewicz, O. C., and Taylor, R.L. (1989). *The Finite Element Method*, Fourth Edition, Volume 1: Basic Formulation and Linear Problems (McGraw-Hill Book Company, London).

Zwislocki, J. (1962). "Analysis of the middle-ear function. Part I: input impedance," *J. Acoust. Soc. Am.* **34**, 1514-1523.

Zwislocki, J., and Feldman, A.S. (1963). "Post-mortem acoustic impedance of human ears," *J. Acoust. Soc. Am.* **35**, 104-107.

# IMAGE EVALUATION TEST TARGET (QA-3)



**APPLIED IMAGE, Inc**  
 1653 East Main Street  
 Rochester, NY 14609 USA  
 Phone: 716/482-0300  
 Fax: 716/288-5989

© 1993, Applied Image, Inc., All Rights Reserved